Directed and elliptic flow in heavy-ion collisions from $E_{\mathrm{beam}} = 90$ MeV/nucleon to $E_{\mathrm{c.m.}} = 200$ GeV/nucleon

Hannah Petersen,[1] Qingfeng Li,[2] Xianglei Zhu,[1,2,3] and Marcus Bleicher[1]

[1]*Institut für Theoretische Physik, Johann Wolfgang Goethe-Universität, Max-von-Laue-Str. 1, D-60438 Frankfurt am Main, Germany*

[2]*Frankfurt Institute for Advanced Studies (FIAS), Max-von-Laue-Str. 1, D-60438 Frankfurt am Main, Germany*

[3]*Physics Department, Tsinghua University, Beijing 100084, People's Republic of China*

(Received 22 August 2006; published 18 December 2006)

Recent data from the NA49 experiment on directed and elliptic flow for Pb+Pb reactions at CERN-SPS are compared to calculations with a hadron-string transport model, the ultrarelativistic quantum molecular dynamics (UrQMD) model. The rapidity and transverse momentum dependence of the directed and elliptic flow, i.e., v_1 and v_2, are investigated. The flow results are compared to data at three different centrality bins. Generally, a reasonable agreement between the data and the calculations is found. Furthermore, the energy excitation functions of v_1 and v_2 from $E_{\mathrm{beam}} = 90A$ MeV to $E_{\mathrm{c.m.}} = 200A$ GeV are explored within the UrQMD framework and discussed in the context of the available data. It is found that, in the energy regime below $E_{\mathrm{beam}} \leqslant 10A$ GeV, the inclusion of nuclear potentials is necessary to describe the data. Above $40A$ GeV beam energy, the UrQMD model starts to underestimate the elliptic flow. Around the same energy the slope of the rapidity spectra of the proton directed flow develops negative values. This effect is known as the third flow component ("antiflow") and cannot be reproduced by the transport model. These differences can possibly be explained by assuming a phase transition from hadron gas to quark gluon plasma at about $40A$ GeV.

DOI: 10.1103/PhysRevC.74.064908 PACS number(s): 25.75.Ld, 25.75.Dw, 25.75.Gz

I. INTRODUCTION

To create extremely hot and dense matter with partons as its fundamental components—called the quark-gluon plasma (QGP)—is a major goal of current and future high-energy heavy-ion collisions experiments at the CERN Super Proton Synchrotron (SPS), BNL Relativistic Heavy Ion Collider (RHIC), and CERN Large Hadron Collider (LHC) [1]. However, due to the complex nature of the relativistic nucleus-nucleus reactions, the QGP, if it has been created, escapes direct detection. Therefore, to establish the existence and later on to investigate the properties of the new state of matter, one must find observables that allow to deduce the properties of the intermediate (QGP) state from the final-state hadrons.

The exploration of the transverse collective flow is the earliest predicted observable to probe heated and compressed nuclear matter [2]. The transverse flow is intimately connected to the pressure gradients. Therefore, it is sensitive to the equation of state (EoS) and might be used to search for abnormal matter states and phase transitions [3–5].

The intermediate energy regime available at CERN-SPS or at the future GSI Facility for Antiproton and Ion Research (GSI-FAIR) facility is often referred to as the right place to look for a phase transition to the QGP. Lattice quantum chromodynamics (lQCD) calculations [6,7] show that the critical temperature is around 170 MeV (for $\mu_b = 0$) and the critical energy density is around 1 GeV/fm^3. These values can already be reached at 20–30A GeV beam energy. At finite baryochemical potential, the heated and compressed nuclear matter created at these energies crosses the phase transition line possibly even on the high μ side of the critical endpoint. Therefore, it is possible to talk about a phase transition of first order here. During such a first-order phase transition the softest point in the equation of state would be mostly pronounced. For example, the proton antiflow around midrapidity ("third flow component" [8]) and the collapse of the elliptic flow observable have been declared as a signal for the phase transition [9,10].

In this article, recent results on proton- and pion-directed and elliptic flow from the NA49 experiment [11] are investigated and predictions for FAIR are presented. The data are compared to transport model calculations (UrQMD v2.2). The proton flow measures the behavior of the nuclear matter during a heavy-ion collision, whereas the flow of pions is a sign for the properties of newly produced particles.

The article is organized as follows. Section II includes an introduction of the UrQMD model. Sections III and IV introduce the flow systematics and the different measurement methods. In Sec. V, the directed flow results are shown. There are rapidity and transverse momentum distributions for 40 and 160A GeV beam energy. The centrality dependence is also studied. Predictions for rapidity and p_t dependence of v_1 for $E_{\mathrm{beam}} = 20$ and $30A$ GeV are made. In Sec. V C the energy dependence of the slope around midrapidity of the directed flow is investigated in the context of the available data. Afterwards, in Sec. VI, the same analysis for the rapidity and transverse-momentum dependence of elliptic flow (v_2) is shown. Section VI C discusses the excitation function of elliptic flow over the whole energy range from GSI Schwerionen Synchrotron (SIS) to RHIC. Section VII summarizes the article.

II. THE UrQMD MODEL

For our investigation, the ultrarelativistic quantum molecular dynamics model (UrQMD v2.2) [12,13] is applied to heavy-ion reactions from $E_{\mathrm{beam}} = 90A$ MeV to $\sqrt{s_{NN}} =$ 200 GeV. This microscopic transport approach is based on

the covariant propagation of constituent quarks and diquarks accompanied by mesonic and baryonic degrees of freedom. It simulates multiple interactions of in-going and newly produced particles, the excitation and fragmentation of color strings and the formation and decay of hadronic resonances. Toward higher energies, the treatment of subhadronic degrees of freedom is of major importance. In the present model, these degrees of freedom enter via the introduction of a formation time for hadrons produced in the fragmentation of strings [14–16]. A phase transition to a quark-gluon state is not incorporated explicitly into the model dynamics. However, a detailed analysis of the model in equilibrium, yields an effective equation of state of Hagedorn type [17,18].

The UrQMD transport model is successful in describing the yields and the p_t spectra of different particles in pp and pA collisions [19]. It has also been applied to study the flow at lower energies and at RHIC energies [20–25].

III. FLOW SYSTEMATICS

The first coefficient of the Fourier expansion of the azimuthal distribution of the emitted particles (v_1) describes the directed in-plane flow. The directed flow measures the total amount of transverse flow. It is most pronounced in semicentral interactions around target and projectile rapidities where the spectators are deflected away from the beam axis due to a bounce-off from the compressed and heated matter in the overlap region. v_1 is defined by

$$v_1 \equiv \langle \cos(\phi - \Phi_{\mathrm{RP}}) \rangle, \tag{1}$$

where ϕ denotes the azimuthal angle of one outgoing particles and Φ_{RP} is the azimuthal angle of the reaction plane. The angular brackets denote an average over all considered particles from all events.

Three different interesting properties of the directed flow have been proposed. (i) The time scales probed by the directed flow are set by the crossing time of the Lorentz-contracted nuclei. Thus, it serves as keyhole to the initial, probably nonequilibrium, stage of the reaction [26]. (ii) The softening of the equation of state in a first-order phase transition leads to a decreasing directed flow [27–29]. (iii) The space-momentum correlation of the emitted particles can be adressed experimentally via the v_1 rapidity distributions of nucleons and pions.

The second coefficient of the Fourier expansion of the azimuthal distribution of the emitted particles (v_2) is called elliptic flow [8,30–39]. This type of flow is strongest around central rapidities in semiperipheral collisions. It is driven by the anisotropy of the pressure *gradients*, due to the geometric anisotropy of the initial overlapping region. Therefore, it is a valuable tool to gain insight into the expanding stage of the fire ball. v_2 is defined by

$$v_2 \equiv \langle \cos[2(\phi - \Phi_{\mathrm{RP}})] \rangle. \tag{2}$$

There are two competing effects that lead to contributions with different signs to the integrated v_2 value. At low energies or early times there is the so-called squeeze-out effect. The spectator matter blocks the emission in the impact parameter direction and therefore the flowing matter is "squeezed out" perpendicularly to the reaction plane. This leads to negative elliptic flow values. The second effect is the so called in-plane flow. This type of flow becomes important at higher energies and/or later times. At higher bombarding energies ($E_{\mathrm{lab}} \geqslant 10A$ GeV) the spectators leave the interaction zone quickly. The remaining hot and dense matter expands almost freely, where the surface is such that in-plane emission is preferred. Therefore the elliptic flow receives a positive contribution.

Let us now explore the time evolution of the pressure gradients in connection with the elliptic flow development. The transverse pressure gradients have been calculated for the first 10 fm at $E_{\mathrm{lab}} = 40A$ GeV (see Fig. 1) and the highest

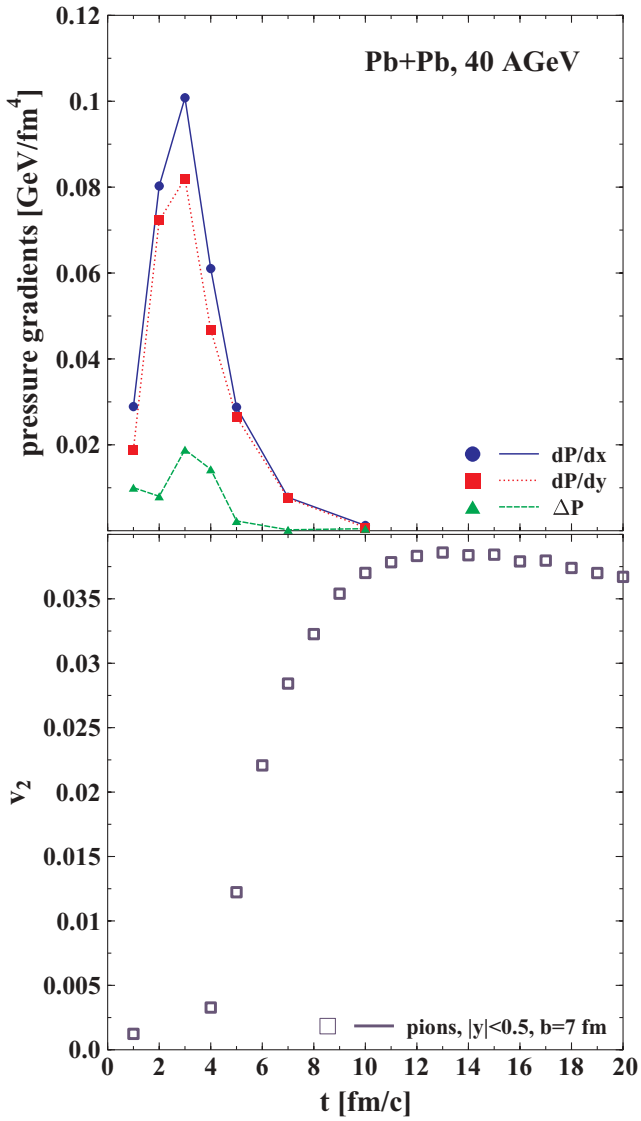

FIG. 1. (Color online) UrQMD calculation for the time evolution of the pressure gradients and elliptic flow for Pb+Pb interactions at $E_{\mathrm{lab}} = 40A$ GeV. (Top) dP/dx (full line), dP/dy (dotted line), and the difference between these two ΔP (dashed line) are depicted. (Bottom) Elliptic flow of pions (squares) versus time at midrapidity for midcentral collisions ($b = 7$ fm).

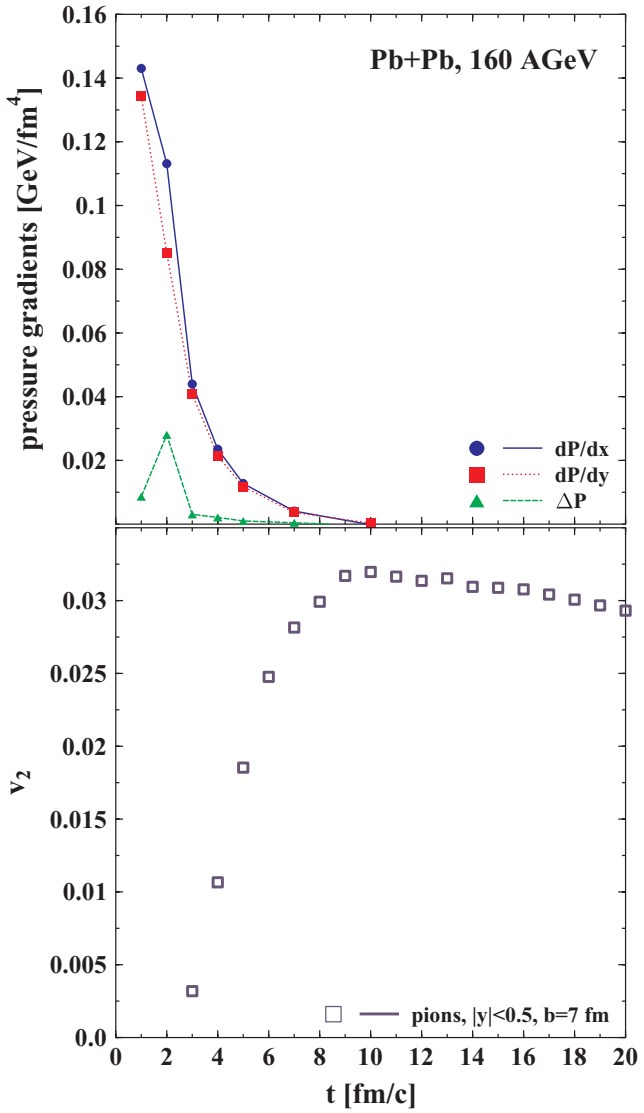

FIG. 2. (Color online) UrQMD calculation for the time evolution of the pressure gradients and elliptic flow for Pb+Pb interactions at $E_{\rm lab} = 160A$ GeV. (Top) dP/dx (full line), dP/dy (dotted line), and the difference between these two ΔP (dashed line) are depicted. (Bottom) Elliptic flow of pions (squares) versus time at midrapidity for midcentral collisions ($b = 7$ fm).

SPS energy (see Fig. 2). In both cases one observes large pressure gradients in the very early stage of the collision. For the lower energy the maximum is reached around $t = 3$ fm and for the higher energy it is shifted to even earlier times. The difference between the pressure gradients in x and y directions is responsible for the v_2 development. As it can be seen in Figs. 1 (bottom) and 2 (bottom) the temporal evolution of elliptic flow for pions starts exactly after this maximum. The elliptic flow increases during ~6 fm until it reaches almost its final value. After $t = 10$ fm it decreases a little because of resonance decays. So, elliptic flow builds up in the early stage of the collision due to the difference of pressure gradients as it is expected.

IV. FLOW MEASUREMENT METHODS

In the UrQMD model calculation of flow, the exact azimuthal angle of the reaction plane $\Phi_{\rm RP}$ is known by definition. However, an unambiguous experimental measurement of the azimuthal anisotropic flow is not a trivial task due to the unknown orientation of the reaction plane. Often, experiments use the so-called reaction plane method [40] to extract the magnitude of flow. In this method, the reaction plane is fixed according to the flow vector of the event, then the estimated v_2 with respect to the chosen reaction plane is corrected for the event plane resolution, which accounts for the error in the deduction of the reaction plane.

However, these two-particle correlations based method might suffer from effects that are not related to the reaction

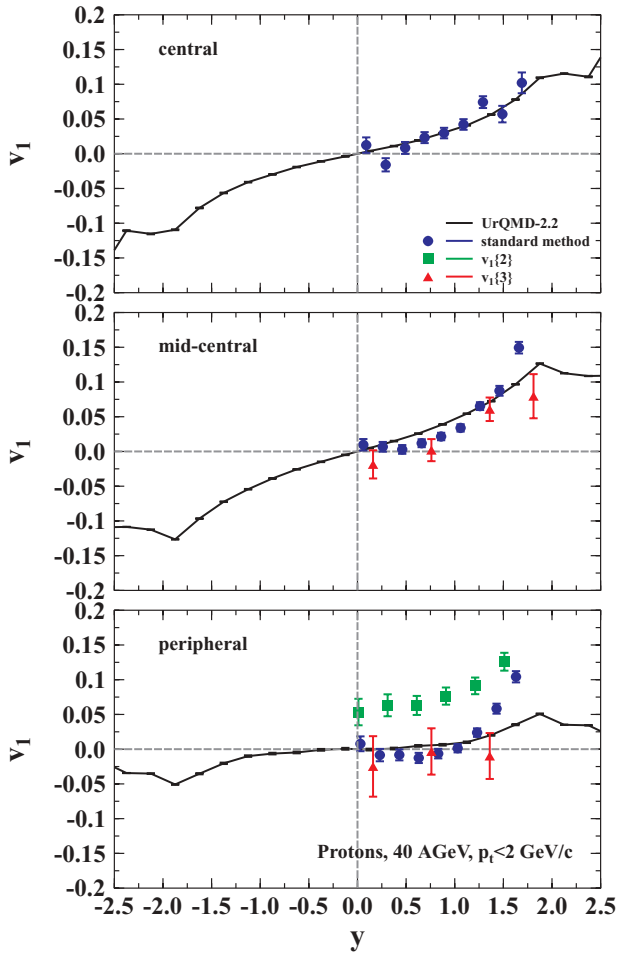

FIG. 3. (Color online) Directed flow of protons in Pb+Pb collisions at $E_{\rm lab} = 40A$ GeV with $p_t < 2$ GeV/c. UrQMD calculations are depicted with black lines. The symbols are NA49 data from different analysis methods. The standard method (circles), cumulant method of order 2 (squares) and cumulant method of order 3 (triangles) are depicted. The 12.5% most central collisions are labeled as central, the centrality 12.5%–33.5% as midcentral and 33.5%–100% as peripheral. For the model calculations the corresponding impact parameters of $b \leqslant 3.4$ fm for central, $b = 5$–9 fm for midcentral, and $b = 9$–15 fm for peripheral collisions have been used.

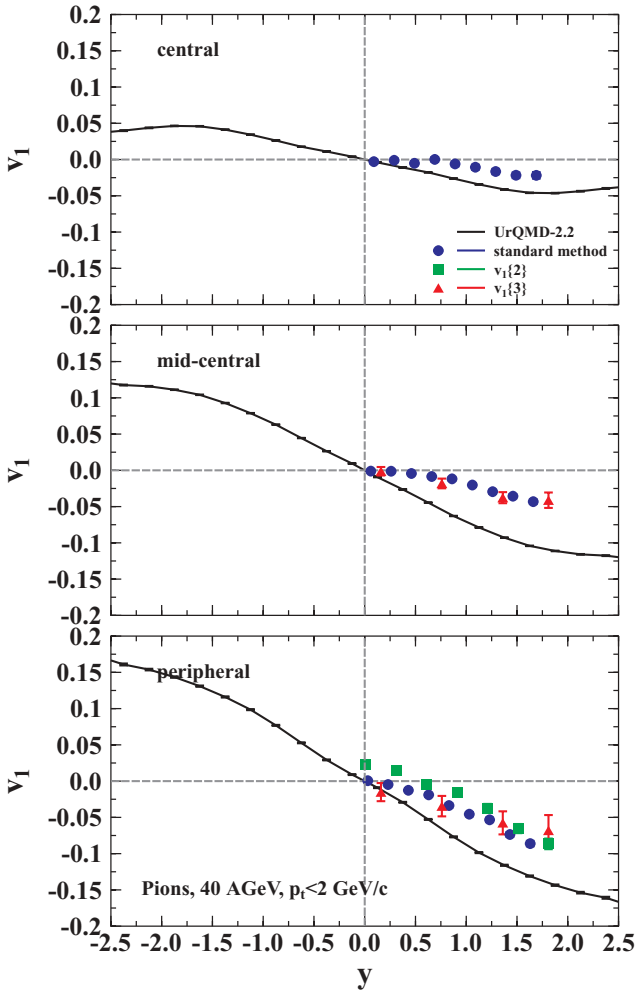

FIG. 4. (Color online) Directed flow of pions in Pb+Pb collisions at $E_{\rm lab} = 40A$ GeV with $p_t < 2$ GeV/c. UrQMD calculations are depicted with black lines. The symbols are NA49 data from different analysis methods. The standard method (circles), cumulant method of order 2 (squares), and cumulant method of order 3 (triangles) are depicted. The 12.5% most central collisions are labeled as central, the centrality 12.5%–33.5% as midcentral and 33.5%–100% as peripheral. For the model calculations the corresponding impact parameters of $b \leqslant 3.4$ fm for central, $b = 5$–9 fm for midcentral and $b = 9$–15 fm for peripheral collisions have been used.

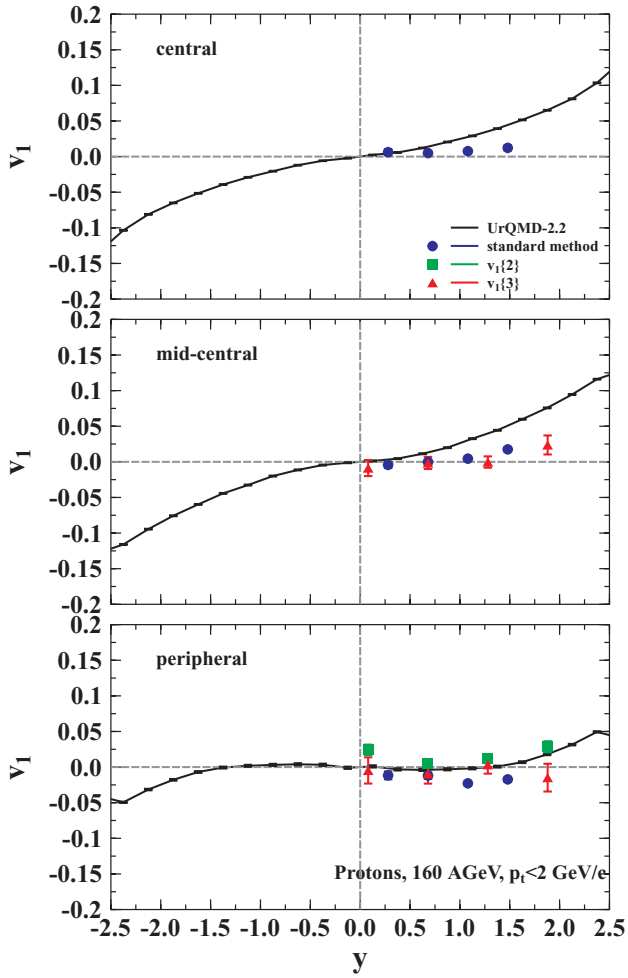

FIG. 5. (Color online) Directed flow of protons in Pb+Pb collisions at $E_{\rm lab} = 160A$ GeV with $p_t < 2$ GeV/c. UrQMD calculations are depicted with black lines. The symbols are NA49 data from different analysis methods. The standard method (circles), cumulant method of order 2 (squares), and cumulant method of order 3 (triangles) are depicted. The 12.5% most central collisions are labeled as central, the centrality 12.5%–33.5% as midcentral and 33.5%–100% as peripheral. For the model calculations the corresponding impact parameters of $b \leqslant 3.4$ fm for central, $b = 5$–9 fm for midcentral, and $b = 9$–15 fm for peripheral collisions have been used.

plane, these additional contributions are usually called nonflow effects [41], such as the overall transverse-momentum conservation, small-angle azimuthal correlations due to final-state interactions, resonance decays, jet production [42], and quantum correlations due to the HBT effect [43]. Recently, the cumulant method was proposed [44,45] to diminish the nonflow effects. The idea of the cumulant method is to extract flow with many-particle cumulants, which are the many-particle correlations with subtraction of the contributions from the correlations due to the lower-order multiplets. It is believed that the pure many-particle nonflow correlations have much less contributions to the measured flow in the many-particle cumulant method. In other words, the many-particle cumulant method should be much less sensitive to nonflow effects [44,45].

This has been confirmed by the test of the cumulant method with the UrQMD model [24,25]. However, the test also shows that, at least for the v_2 measurement, the cumulant method is not completely free from the effect of event-by-event v_2 fluctuations [46]. Especially when the genuine v_2 signal is weak (for example, for the most central events and very peripheral events), the effect of v_2 fluctuations could be so strong that the results from the cumulant method becomes unreliable.

V. DIRECTED FLOW RESULTS

A. Rapidity dependence

Figure 3 shows the rapidity dependence of the directed flow of protons for central ($b \leqslant 3.4$ fm), midcentral ($b = 5$–9 fm),

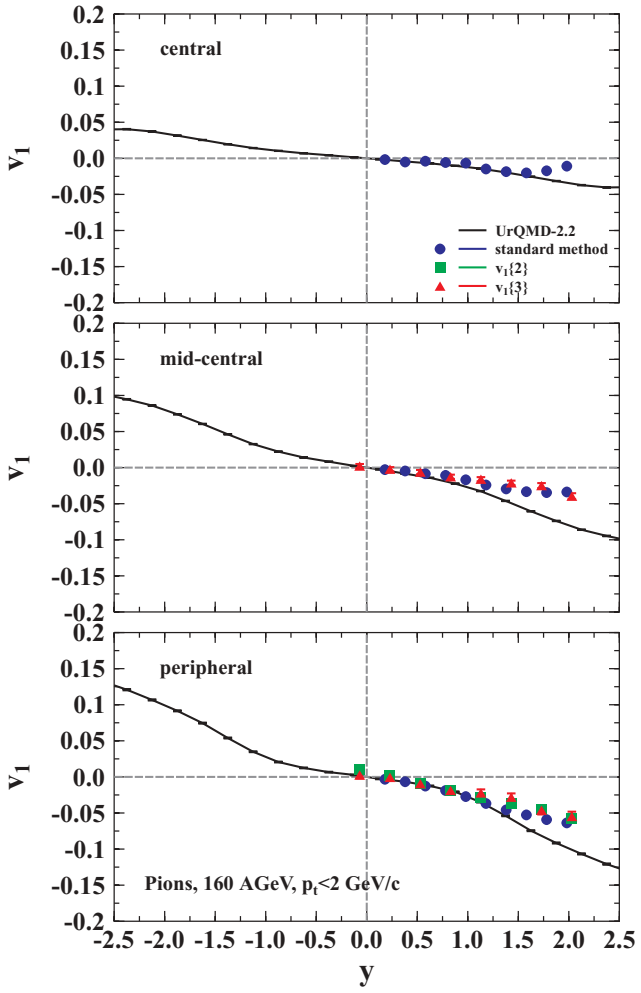

FIG. 6. (Color online) Directed flow of pions in Pb+Pb collisions at $E_{\rm lab} = 160A$ GeV with $p_t < 2$ GeV/c. UrQMD calculations are depicted with black lines. The symbols are NA49 data from different analysis methods. The standard method (circles), cumulant method of order 2 (squares), and cumulant method of order 3 (triangles) are depicted. The 12.5% most central collisions are labeled as central, the centrality 12.5%–33.5% as midcentral, and 33.5%–100% as peripheral. For the model calculations the corresponding impact parameters of $b \leqslant 3.4$ fm for central, $b = 5$–9 fm for midcentral, and $b = 9$–15 fm for peripheral collisions have been used.

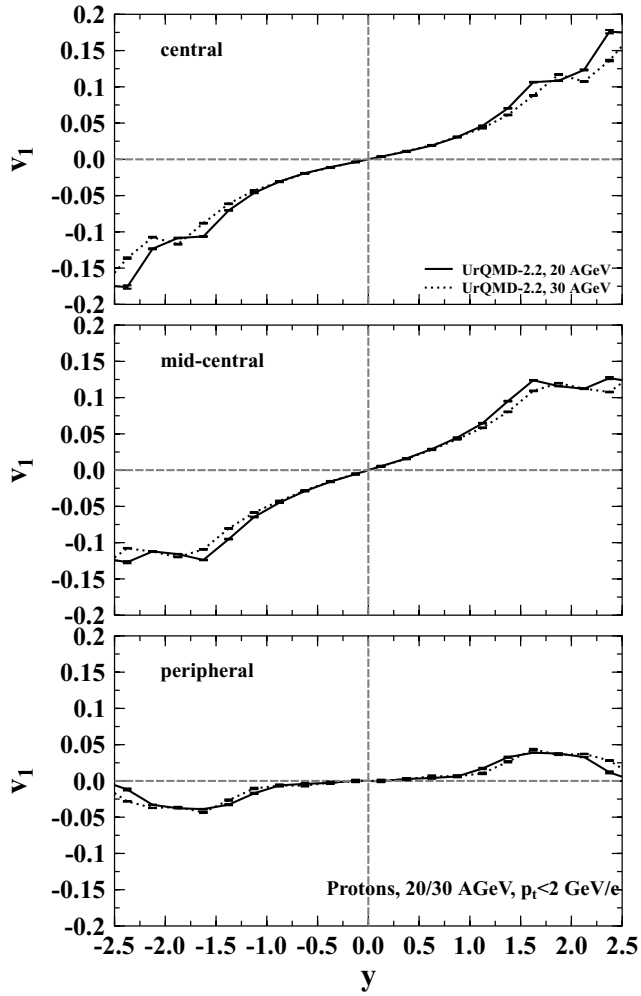

FIG. 7. Directed flow of protons in Pb+Pb collisions at $E_{\rm lab} = 20A$ GeV and $E_{\rm lab} = 30A$ GeV with $p_t < 2$ GeV/c. UrQMD calculations for $20A$ GeV are depicted with solid lines, whereas the results for $30A$ GeV are depicted by dashed lines. Impact parameters of $b \leqslant 3.4$ fm for central, $b = 5$–9 fm for midcentral, and $b = 9$–15 fm for peripheral collisions have been used.

and peripheral ($b \geqslant 9$ fm) Pb+Pb reactions at $E_{\rm lab} = 40A$ GeV. The symbols denote data by the NA49 Collaboration analyzed with different methods [11]. UrQMD calculations are depicted with black lines. The directed flow is most pronounced at high rapidity values where the bounced-off spectator matter sits.

The strong centrality dependence of v_1 can be seen, as the shape of the curves changes drastically from central to peripheral collisions. Overall, the model calculations are in line with the data from the event plane method (standard method, full circle). It is interesting to note that one kind of nonflow effects, i.e., momentum conservation, has been subtracted in this reaction plane method already [47]. Unfortunately, the two-particle cumulant measurements seem to be affected by the nonflow effects that are in this analysis dominated by momentum conservation. This effect is most pronounced for peripheral collisions. Here, the experimental data points do not approach zero at midrapidity. For the more reliable three-particle cumulant method [48], the experimental results agree well with those of the reaction plane method within the statistical error (please see also the following v_1 data). This indicates that the momentum conservation corrected reaction plane method gives also reliable v_1 data.

Figure 4 shows directed flow of pions at $E_{\rm lab} = 40A$ GeV. The different sign with respect to the proton flow can be explained by shadowing. The pions are newly produced mesons and therefore they are composed by a quark and especially an antiquark. Therefore, the cross section of the pions with the nuclear matter is so large that they cannot escape in the direction where the rest of the colliding nuclei/spectator matter resides.

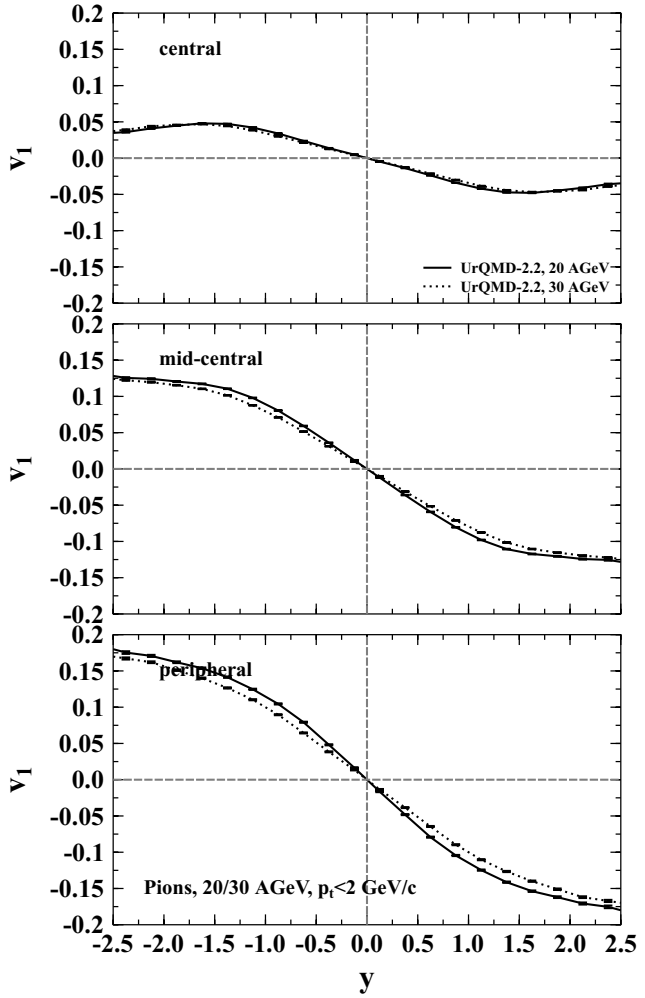

FIG. 8. Directed flow of pions in Pb+Pb collisions at $E_{\text{lab}} = 20A$ GeV and $E_{\text{lab}} = 30A$ GeV with $p_t < 2$ GeV/c. UrQMD calculations for $20A$ GeV are depicted with solid lines, whereas the results for $30A$ GeV are depicted by dashed lines. Impact parameters of $b \leqslant 3.4$ fm for central, $b = 5$–9 fm for midcentral, and $b = 9$–15 fm for peripheral collisions have been used.

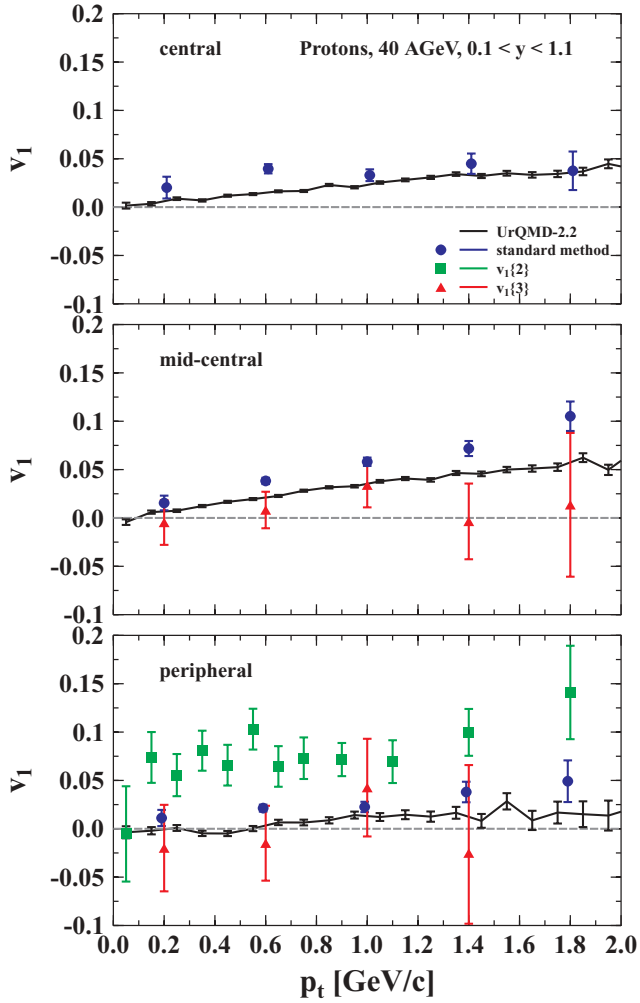

FIG. 9. (Color online) Directed flow of protons in Pb+Pb collisions at $E_{\text{lab}} = 40A$ GeV with $0.1 < y < 1.1$. UrQMD calculations are depicted with black lines. The symbols are NA49 data from different analysis methods. The standard method (circles), cumulant method of order 2 (squares), and cumulant method of order 3 (triangles) are depicted. The 12.5%% most central collisions are labeled as central, the centrality 12.5%–33.5% as midcentral, and 33.5%–100% as peripheral. For the model calculations the corresponding impact parameters of $b \leqslant 3.4$ fm for central, $b = 5$–9 fm for midcentral, and $b = 9$–15 fm for peripheral collisions have been used.

For peripheral collisions the measured directed flow reaches the same amount as for protons (about 10% at $y \approx 2$), but for central collisions it is much less (only about 2.5% at $y \approx 2$). The UrQMD calculations overestimate the pion directed flow at large rapidities by about a factor of 2 for all centralities. This overestimation might be explainable if one assumes that the NA49 Collaboration is not able to measure all produced pions. Especially pions produced from nucleons that fly straight ahead through the collision producing only one or two pions appear only in the veto calorimeter. However, in the model calculations every produced pion within the given rapidity and transverse-momentum bin is taken into account.

In Fig. 5, directed flow of protons at $E_{\text{lab}} = 160A$ GeV is shown. In this case the model calculations slightly overestimate the flow at higher rapidities in contrast to the proton flow at $E_{\text{lab}} = 40A$ GeV. Surprisingly, the data stay almost constant at zero. Even in peripheral collisions there are only about $v_1 = 2.5\%$ at $y = 1.5$ for the reaction plane method analysis. The flat shape of the curve with respect to the lower-energy results can be explained by the spectators sit at higher rapidity values in this plot. This spectator matter is responsible for the directed flow near beam/target rapidities. Because there are no data points of the reaction plane method above $y = 1.5$ this increase is not seen.

For the pion-directed flow at the higher SPS energy (Fig. 6), one observes a reasonable agreement between the model calculations and the data from all three measurement methods, i.e., reaction plane method, $v_1\{2\}$ and $v_1\{3\}$. Above $y = 1$, the UrQMD results increase slightly stronger than the data. The centrality dependence is reproduced correctly. Both in the

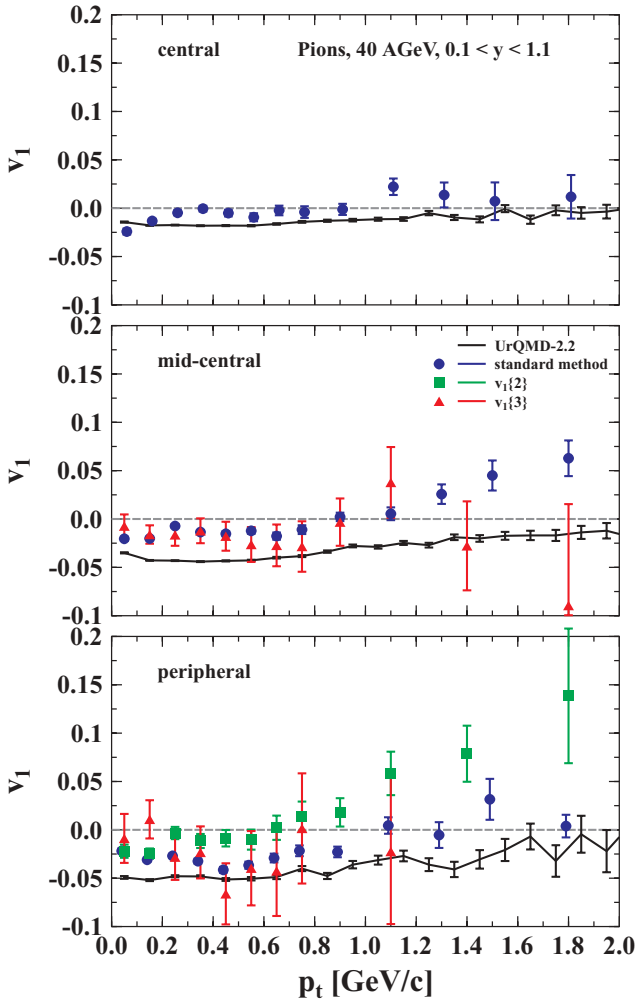

FIG. 10. (Color online) Directed flow of pions in Pb+Pb collisions at $E_{\mathrm{lab}} = 40A$ GeV with $0.1 < y < 1.1$. UrQMD calculations are depicted with black lines. The symbols are NA49 data from different analysis methods. The standard method (circles), cumulant method of order 2 (squares), and cumulant method of order 3 (triangles) are depicted. The 12.5% most central collisions are labeled as central, the centrality 12.5%–33.5% as midcentral, and 33.5%–100% as peripheral. For the model calculations the corresponding impact parameters of $b \leqslant 3.4$ fm for central, $b = 5$–9 fm for midcentral, and $b = 9$–15 fm for peripheral collisions have been used.

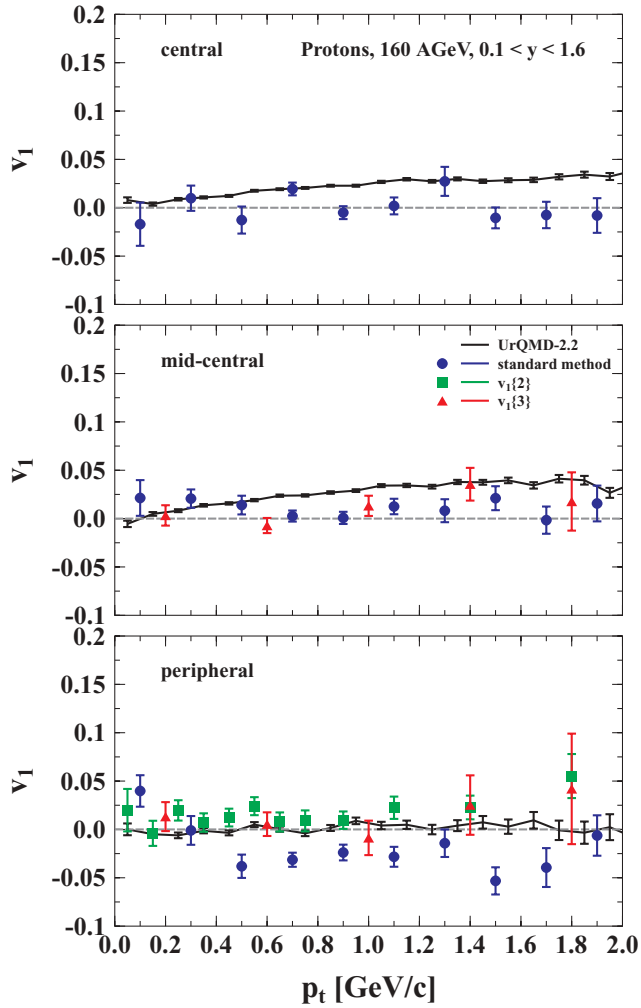

FIG. 11. (Color online) Directed flow of protons in Pb+Pb collisions at $E_{\mathrm{lab}} = 160A$ GeV with $0.1 < y < 1.6$. UrQMD calculations are depicted with black lines. The symbols are NA49 data from different analysis methods. The standard method (circles), cumulant method of order 2 (squares), and cumulant method of order 3 (triangles) are depicted. The 12.5% most central collisions are labeled as central, the centrality 12.5%–33.5% as midcentral, and 33.5%–100% as peripheral. For the model calculations the corresponding impact parameters of $b \leqslant 3.4$ fm for central, $b = 5$–9 fm for midcentral, and $b = 9$–15 fm for peripheral collisions have been used.

model and in the experimental data there is an increase in flow for more peripheral collisions.

Figures 7 and 8 are predictions for the rapidity dependence of proton and pion directed flow at $E_{\mathrm{lab}} = 20A$ GeV and $E_{\mathrm{lab}} = 30A$ GeV. The shown results are calculated using the UrQMD model with a transverse-momentum cut of $p_t < 2$ GeV/c. In the present model, the calculated directed flow results at these energies under investigation at the new FAIR facility at GSI look rather similar to that at $E_{\mathrm{lab}} = 40A$ GeV. There is also an inverse centrality dependence for protons and pions in the amount of the directed flow. It is very interesting to see if the experimental proton flow data at this energy will show the negative slope around midrapidity as predicted.

B. Transverse-momentum dependence

Figure 9 shows directed flow of protons at $E_{\mathrm{lab}} = 40A$ GeV as a function of transverse momentum. For the calculation the same rapidity cut ($0.1 < y < 1.1$) as in the data obtained with the cumulant method has been used. For the standard reaction-plane analysis the different cut of $0.1 < y < 1.8$ has been applied. The different cuts have been used by the experimental collaboration to improve the statistics and reduce the time amount for the analysis. Because the higher-order cumulant method measurements are the most reliable way to reduce systematic errors [24,25], the comparisons are done with the cuts for the cumulant method. The calculations are in line with the $v_1\{3\}$ data for midcentral and peripheral collisions.

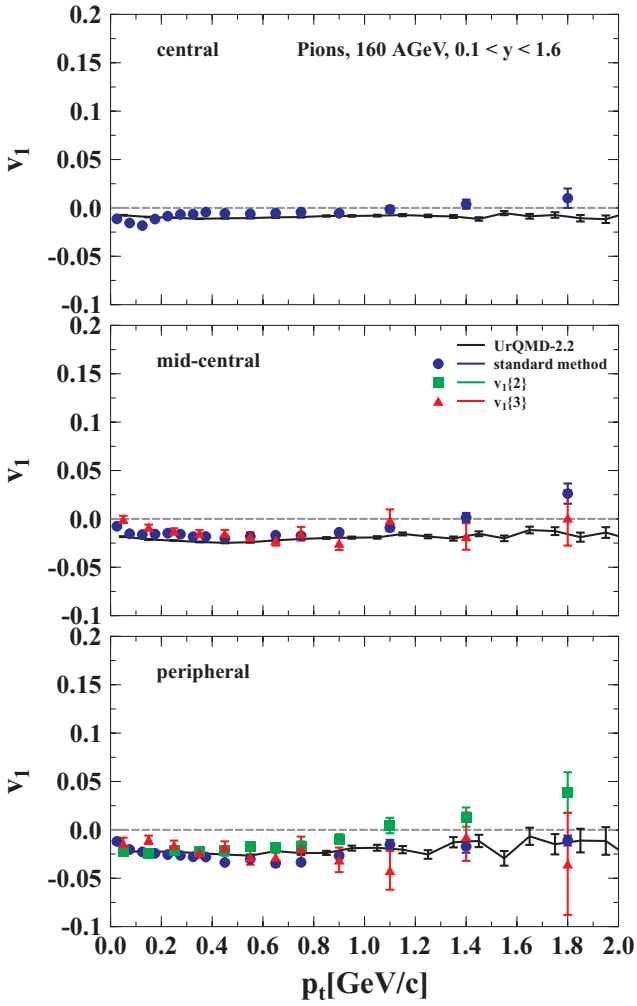

FIG. 12. (Color online) Directed flow of pions in Pb+Pb collisions at $E_{\text{lab}} = 160A$ GeV with $0.1 < y < 1.6$. UrQMD calculations are depicted with black lines. The symbols are NA49 data from different analysis methods. The standard method (circles), cumulant method of order 2 (squares), and cumulant method of order 3 (triangles) are depicted. The 12.5% most central collisions are labeled as central, the centrality 12.5%–33.5% as midcentral, and 33.5%–100% as peripheral. For the model calculations the corresponding impact parameters of $b \leqslant 3.4$ fm for central, $b = 5$–9 fm for midcentral, and $b = 9$–15 fm for peripheral collisions have been used.

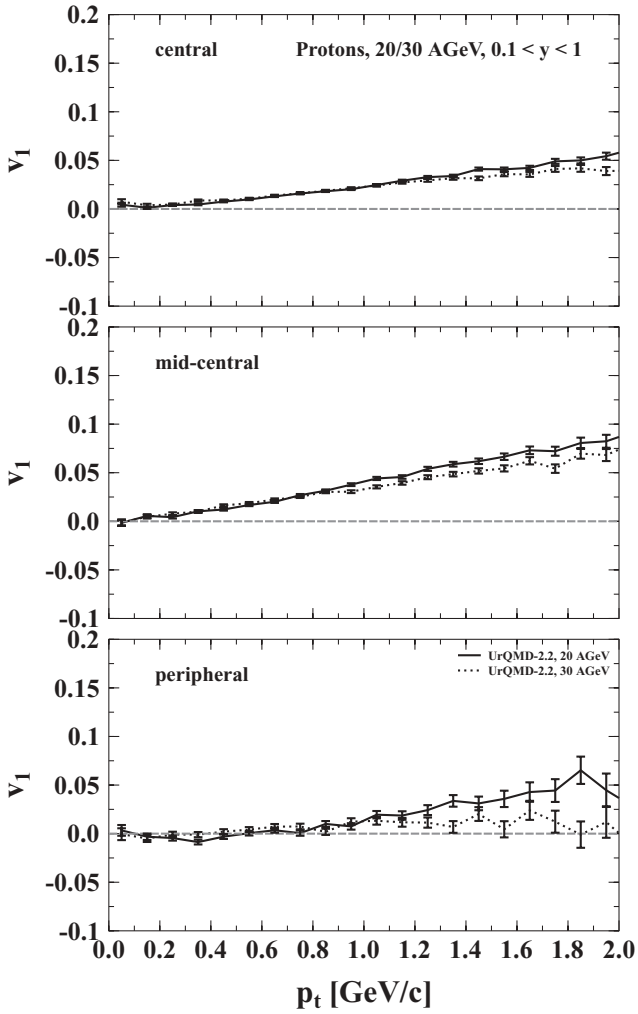

FIG. 13. Directed flow of protons in Pb+Pb collisions at $E_{\text{lab}} = 20A$ GeV and $E_{\text{lab}} = 30A$ GeV with $0.1 < y < 1$. UrQMD calculations for $20A$ GeV are depicted with solid lines, whereas the results for $30A$ GeV are depicted by dashed lines. Impact parameters of $b \leqslant 3.4$ fm for central, $b = 5$–9 fm for midcentral, and $b = 9$–15 fm for peripheral collisions have been used.

Unfortunately, the statistical errors are the biggest for this method and there are only a few data points because it is the newest and most elaborate analysis.

The transverse-momentum dependence of the pion directed flow at $E_{\text{lab}} = 40A$ GeV (Fig. 10) shows many uncertainties. The data differ very much depending on the analysis method. Furthermore, the cumulant method of order 3 has large statistical error bars. The UrQMD calculations are negative as the sign convention suggests. It is remarkable that the directed flow does not show any clear transverse-momentum dependence.

Next, we turn to the results for $160A$ GeV collisions. For central collisions the calculated transverse-momentum dependence of the directed flow of protons at $E_{\text{lab}} = 160A$ GeV (see Fig. 11) starts at zero for $p_t = 0$ and increases steadily until 2% at $p_t = 2$ GeV/c. The measured data fluctuates between +2% and −2%. Going to midcentral collisions the calculations are quite in line with the third-order cumulant method and the standard method data. In peripheral collisions there are big systematic uncertainties because especially around $p_t = 1.8$ GeV/c the data points differ between −4% and +5.5%. The second-order cumulant results are higher, but they are not corrected due to momentum conservation. The negative directed flow of protons is consistent with the rapidity distribution. Because of the negative slope around midrapidity at the higher SPS energy the protons fly in the "wrong" direction.

The calculated directed flow for pions at $E_{\text{lab}} = 160A$ GeV, as depicted in Fig. 12, stays constant as a function of the transverse momentum at (−1)% for central, at (−2)%

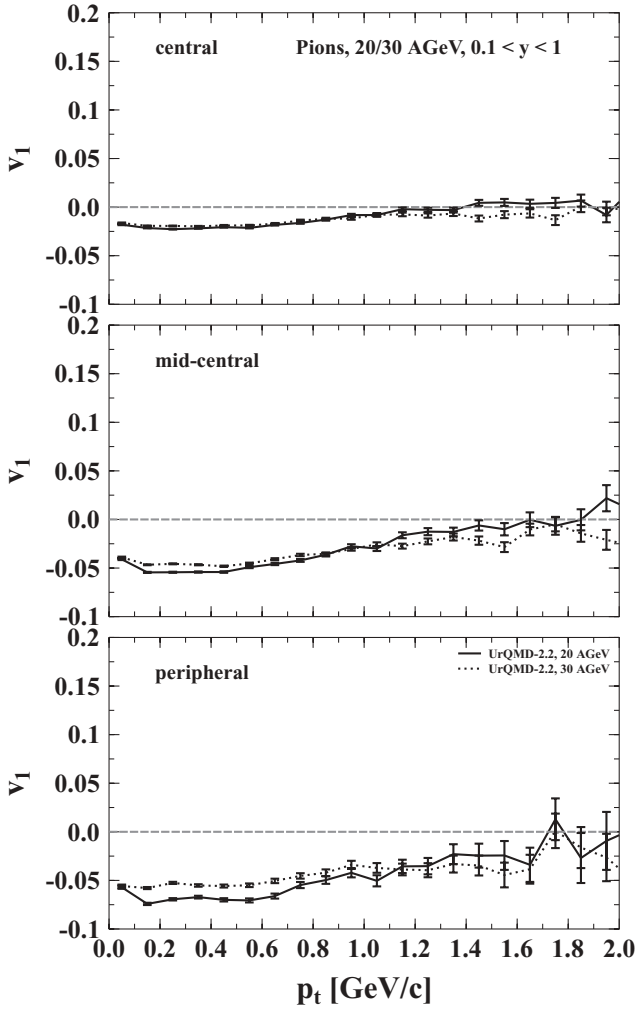

FIG. 14. Directed flow of pions in Pb+Pb collisions at $E_{\rm lab} = 20A$ GeV and $E_{\rm lab} = 30A$ GeV with $0.1 < y < 1$. UrQMD calculations for $20A$ GeV are depicted with solid lines, whereas the results for $30A$ GeV are depicted by dashed lines. Impact parameters of $b \leqslant 3.4$ fm for central, $b = 5$–9 fm for midcentral, and $b = 9$–15 fm for peripheral collisions have been used.

for midcentral, and at $(-3)\%$ for peripheral collisions. In midcentral and peripheral collisions this trend is in line with the third-order cumulant measurement. Especially the data from second-order cumulant increase up to 4%–6%. This is probably due to momentum conservation that is not taken into account to correct the data. The negative directed flow of pions is consistent with the rapidity dependence in the chosen bin.

Finally, we show the prediction for the transverse-momentum dependence of directed flow at $E_{\rm lab} = 20A$ GeV and $E_{\rm lab} = 30A$ GeV in Figs. 13 and 14. In the present calculations, the shape and magnitude of the flow are similar to the results at $40A$ GeV. The directed flow of pions at $20A$ GeV and $30A$ GeV looks also rather similar to the calculations for the pion directed flow at $40A$ GeV. But there is a difference for peripheral collisions. The $v_1(p_t)$ value is only about $(-2.5)\%$ compared to $(-5)\%$ at $E_{\rm lab} = 40A$ GeV.

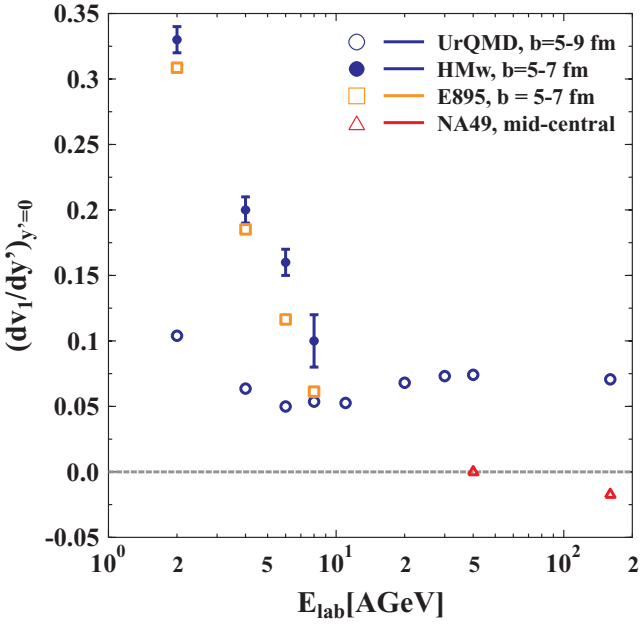

FIG. 15. (Color online) Slope of $v_1(y)$ of protons around midrapidity extracted from normalized ($y' = y/y_b$) rapidity distributions. The data are taken from E895 (squares) [49] and NA49 (triangles) [11]. UrQMD calculations with included mean field (HMw) are depicted with filled circles. Open circles depict UrQMD calculation in the cascade mode.

C. Excitation function

To characterize the amount and the direction of the directed flow of protons over the energy range from $2A$ GeV to $160A$ GeV one can extract the slope around midrapidity from the normalized rapidity distributions usually referred to as the F parameter [49]. "Normalized" means in this case y/y_b, where y_b is the beam rapidity. This normalization accounts for the trivial energy dependence of the slope. The values for the slope in Fig. 15 have been extracted via a polynomial fit of the form $ax + bx^3$ with $x = y/y_b$. At low energies, one observes that the inclusion of a nuclear potential is needed to reproduce the data. Here is shown the calculation with included mean field from a hard equation of state with momentum dependence and medium-modified nucleon-nucleon cross sections (HMw) [50,51]. At higher energies the calculation has been performed in the cacsade mode without the additional inclusion of nuclear potentials.

At SPS energies the data develop even negative values for the slope around midrapidity [9,10]. This behavior cannot be reproduced within the transport model calculation. However, ideal hydro calculations have predicted the appearance of a so-called third flow component [8] or antiflow [52] at finite impact parameters. In these analysis it was pointed out that this antiflow develops if the matter undergoes a first-order phase transition to the QGP. In contrast, a hadronic equation of state without QGP phase transition did not yield such an exotic antiflow (negative slope) wiggle in the proton flow $v_1(y)$ at low energies.

VI. ELLIPTIC FLOW

A. Rapidity dependence

Elliptic flow develops because of the almond shape of the overlapping region in a heavy-ion collision. The breakdown of proton elliptic flow at $E_{\rm lab} = 40A$ GeV has been stressed as a signal for the observation of a first-order phase transition [10]. As can be seen from the NA49 data in Fig. 16, the elliptic flow parameter v_2 vanishes at midrapidity only for the standard reaction plane method data, which could be affected by the nonflow effects. The cumulant measurements show a completely different shape. The second- and fourth-order v_2 measurements for peripheral and midcentral collisions

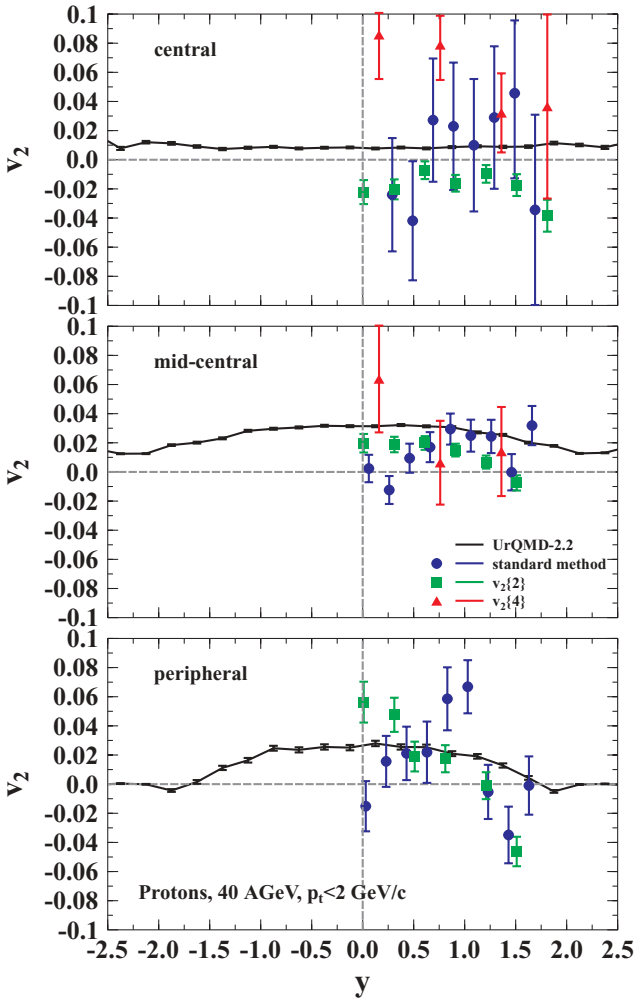

FIG. 16. (Color online) Elliptic flow of protons in Pb+Pb collisions at $E_{\rm lab} = 40A$ GeV with $p_t < 2$ GeV/c. UrQMD calculations are depicted with black lines. The symbols are NA49 data from different analysis methods. The standard method (circles), cumulant method of order 2 (squares), and cumulant method of order 3 (triangles) are depicted. The 12.5% most central collisions are labeled as central, the centrality 12.5%–33.5% as midcentral and 33.5%–100% as peripheral. For the model calculations the corresponding impact parameters of $b \leqslant 3.4$ fm for central, $b = 5$–9 fm for midcentral, and $b = 9$–15 fm for peripheral collisions have been used.

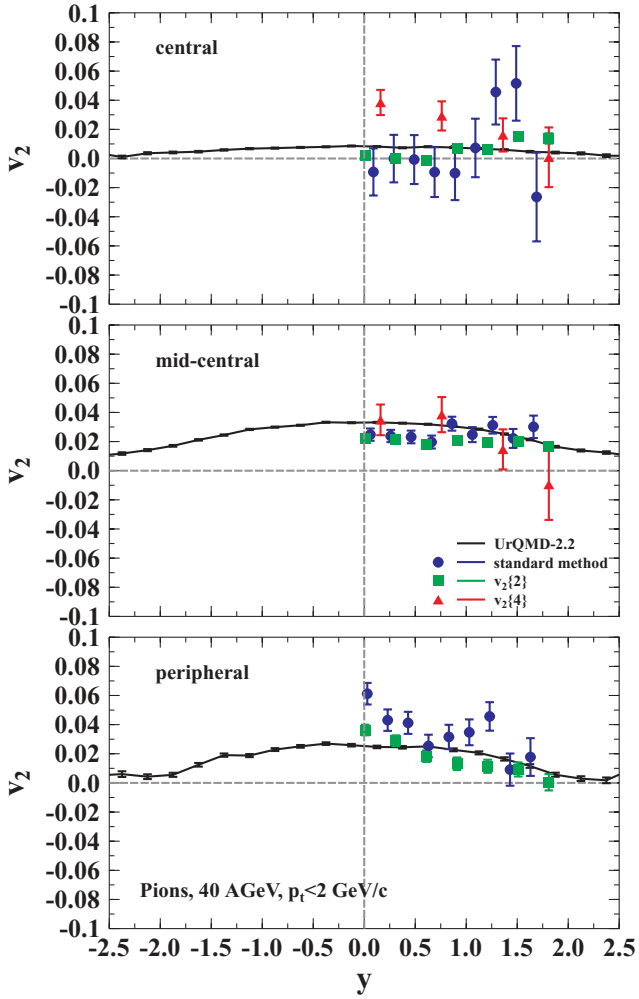

FIG. 17. (Color online) Elliptic flow of pions in Pb+Pb collisions at $E_{\rm lab} = 40A$ GeV with $p_t < 2$ GeV/c. UrQMD calculations are depicted with black lines. The symbols are NA49 data from different analysis methods. The standard method (circles), cumulant method of order 2 (squares), and cumulant method of order 3 (triangles) are depicted. The 12.5% most central collisions are labeled as central, the centrality 12.5%–33.5% as midcentral, and 33.5%–100% as peripheral. For the model calculations the corresponding impact parameters of $b \leqslant 3.4$ fm for central, $b = 5$–9 fm for midcentral, and $b = 9$–15 fm for peripheral collisions have been used.

increase to about 6%–8% around midrapidity not consistent with zero. Looking now at the UrQMD calculations one cannot observe an overestimation but finds that the results are compatible with the data. Therefore, before one can draw concise conclusions the systematic and statistical uncertainties of the data must be resolved.

For the elliptic flow of pions (Fig. 17) in central collisions there are again systematic uncertainties in the experimental data. Again all three methods have different shapes and the calculated elliptic flow value is consistent with the measurement with errors. The elliptic flow increases to about 1% around midrapidity within the UrQMD model. For midcentral collisions the picture becomes clearer. The data

and the calculations are in line. Here, the elliptic flow around midrapidity is about 2%–3%. Going to peripheral collisions the experimental results of the standard method show an unsteady behavior but are compatible with the UrQMD calculations.

The elliptic flow is expected to be larger in more peripheral collisions because the anisotropy in coordinate space that is the source of this flow component is larger. This dependence can be seen very well in the proton flow at $E_{\rm lab} = 160A$ GeV (Fig. 18). In central collisions there is almost no elliptic flow at all. Going to midcentral collisions the flow is between 2% and 6% depending on rapidity and in peripheral collisions even between 2 and 8%. The model calculations do not show a big

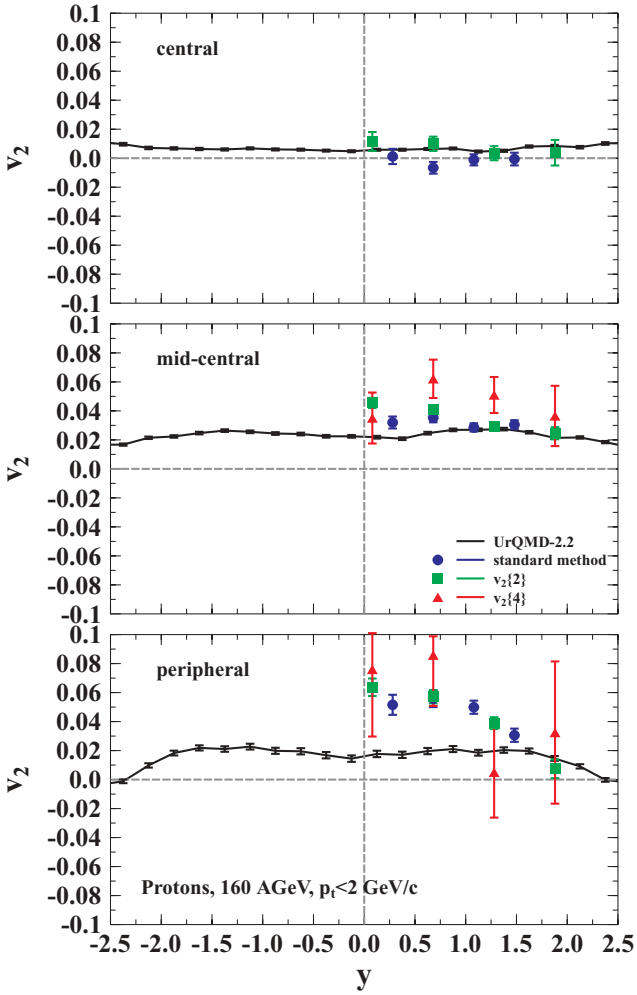

FIG. 18. (Color online) Elliptic flow of protons in Pb+Pb collisions at $E_{\rm lab} = 160A$ GeV with $p_t < 2$ GeV/c. UrQMD calculations are depicted with black lines. The symbols are NA49 data from different analysis methods. The standard method (circles), cumulant method of order 2 (squares), and cumulant method of order 3 (triangles) are depicted. The 12.5% most central collisions are labeled as central, the centrality 12.5%–33.5% as midcentral, and 33.5%–100% as peripheral. For the model calculations the corresponding impact parameters of $b \leqslant 3.4$ fm for central, $b = 5$–9 fm for midcentral, and $b = 9$–15 fm for peripheral collisions have been used.

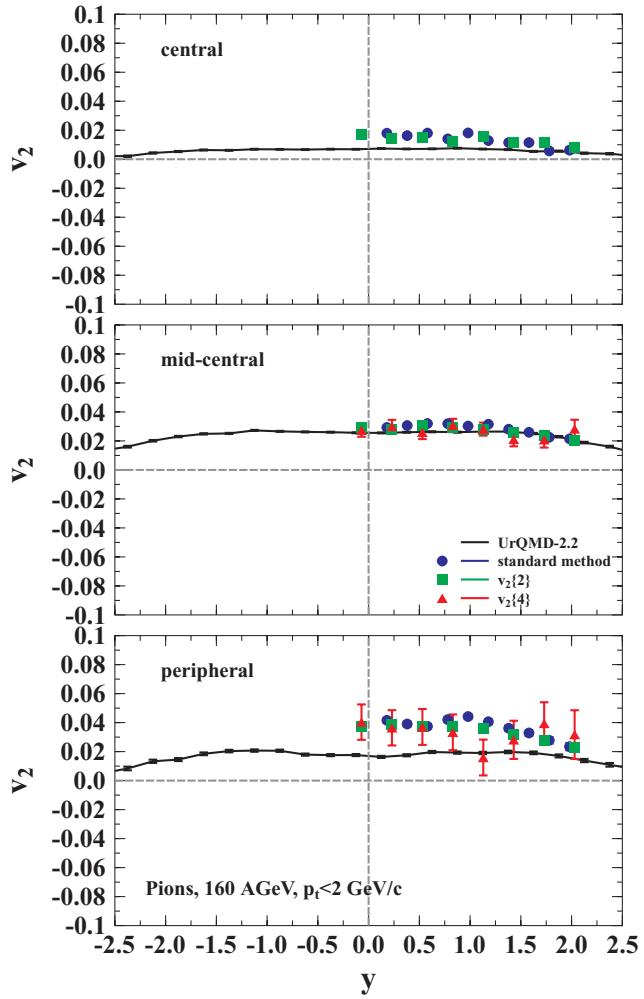

FIG. 19. (Color online) Elliptic flow of pions in Pb+Pb collisions at $E_{\rm lab} = 160A$ GeV with $p_t < 2$ GeV/c. UrQMD calculations are depicted with black lines. The symbols are NA49 data from different analysis methods. The standard method (circles), cumulant method of order 2 (squares), and cumulant method of order 3 (triangles) are depicted. The 12.5% most central collisions are labeled as central, the centrality 12.5%–33.5% as midcentral, and 33.5%–100% as peripheral. For the model calculations the corresponding impact parameters of $b \leqslant 3.4$ fm for central, $b = 5$–9 fm for midcentral, and $b = 9$–15 fm for peripheral collisions have been used.

difference between midcentral and peripheral collisions. Both values are about 2% around midrapidity. The large elliptic flow data in peripheral collisions could be due to the fact of nonflow effects and/or large event-by-event v_2 fluctuations there, which affect the v_2 measurement heavily.

Figure 19 shows the elliptic flow of pions at $E_{\rm lab} = 160A$ GeV. These newly produced particles show almost no elliptic flow in central collisions, i.e., they are emitted isotropically out of the collision region. The experimental result is between 1% and 2%. In midcentral collisions there is a very good agreement between the model and data again. For peripheral collisions the same underestimation of the

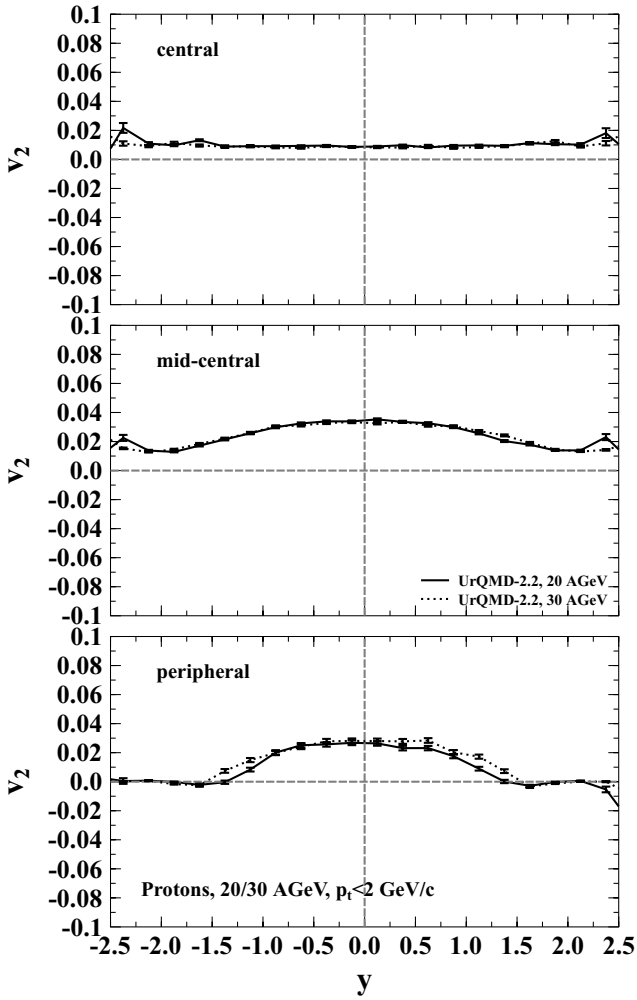

FIG. 20. Elliptic flow of protons in Pb+Pb collisions at $E_{\rm lab} = 20A$ GeV and $E_{\rm lab} = 30A$ GeV with $p_t < 2$ GeV/c. UrQMD calculations for 20A GeV are depicted with solid lines, whereas the results for 30A GeV are depicted by dashed lines. Impact parameters of $b \leqslant 3.4$ fm for central, $b = 5$–9 fm for midcentral, and $b = 9$–15 fm for peripheral collisions have been used.

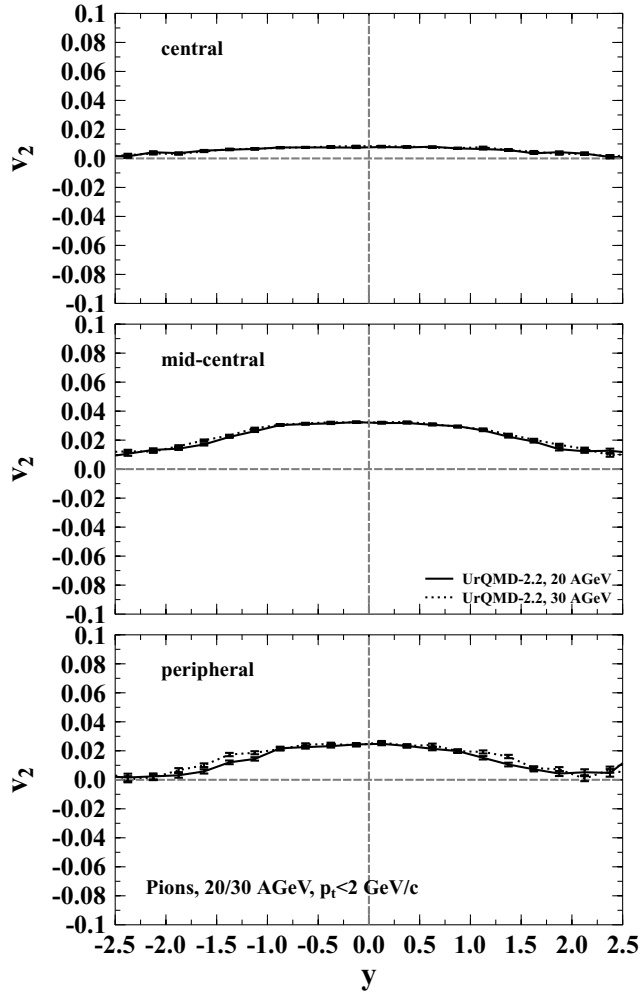

FIG. 21. Elliptic flow of pions in Pb+Pb collisions at $E_{\rm lab} = 20A$ GeV and $E_{\rm lab} = 30A$ GeV with $p_t < 2$ GeV/c. UrQMD calculations for 20A GeV are depicted with solid lines, whereas the results for 30A GeV are depicted by dashed lines. Impact parameters of $b \leqslant 3.4$ fm for central, $b = 5$–9 fm for midcentral, and $b = 9$–15 fm for peripheral collisions have been used.

calculations as for the proton flow in comparison to the data can be seen.

Figures 20 and 21 are predictions for the rapidity dependence of proton and pion elliptic flow at $E_{\rm lab} = 20A$ GeV and $E_{\rm lab} = 30A$ GeV. The shown results are calculated using the UrQMD model with a transverse-momentum cut of $p_t < 2$ GeV/c. The elliptic flow results at this energy of the new accelerator at FAIR at the GSI look rather similar to that at $E_{\rm lab} = 40A$ GeV.

B. Transverse-momentum dependence

For the elliptic flow of protons as a function of transverse momentum there is a different rapidity cut used in the data than in the calculations. For proton and pion flow at $E_{\rm lab} = 40A$ GeV it is $-0.1 < y < 1.1$ and for $E_{\rm lab} = 160A$ GeV it is $0.1 < y < 1.6$ for the cumulant order measurements. For the standard reaction plane method data, larger rapidity bins have been used for the integration. To improve the statistics of the UrQMD results we use symmetric rapidity cuts as $|y| < 1.1$ for 40A GeV and $|y| < 1.6$ for 160A GeV. Because the elliptic flow is symmetric in rapidity this can be done without problems. The elliptic flow of protons at $E_{\rm lab} = 40A$ GeV (Fig. 22) increases only to about 3% for central and peripheral collisions in the calculated results. For midcentral collisions there is a steady increase with the increase of transverse momentum to about 10%, which is in line with the data.

For the calculated pion elliptic flow at $E_{\rm lab} = 40A$ GeV (Fig. 23) a quite similar behavior as for protons is seen. At high p_t the experimental results have large statistical error bars. At low p_t the experimental is not plagued by statistical and systematic errors and one observes good agreement between model and data. There is a increase of elliptic flow

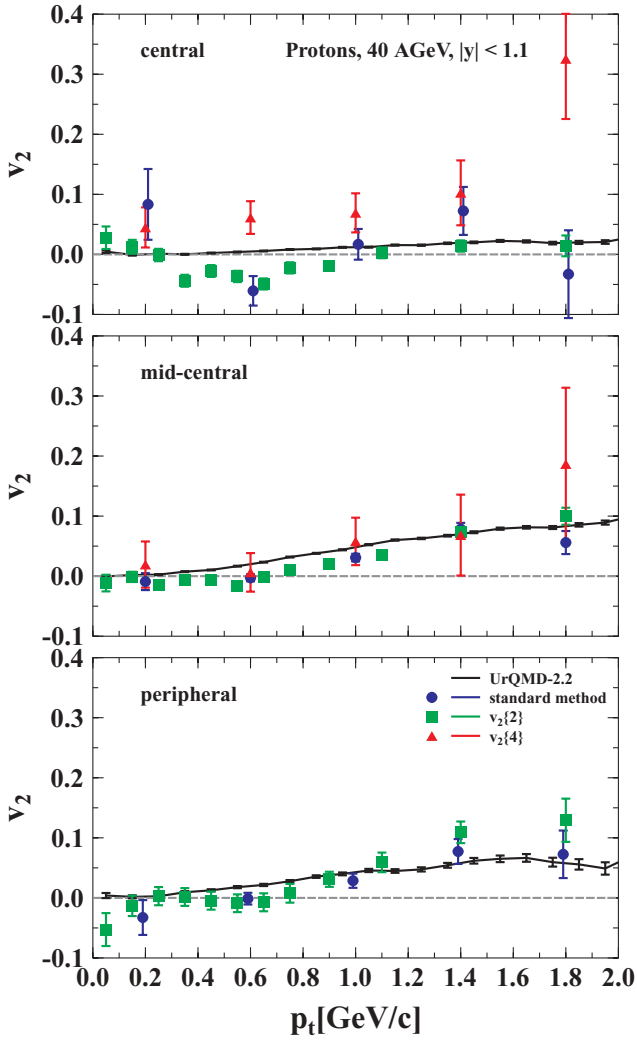

FIG. 22. (Color online) Elliptic flow of protons in Pb+Pb collisions at $E_{\rm lab} = 160A$ GeV with $|y| < 1.1$. UrQMD calculations are depicted with black lines. The symbols are NA49 data from different analysis methods. The standard method (circles), cumulant method of order 2 (squares), and cumulant method of order 3 (triangles) are depicted. The 12.5% most central collisions are labeled as central, the centrality 12.5%–33.5% as midcentral, and 33.5%–100% as peripheral. For the model calculations the corresponding impact parameters of $b \leqslant 3.4$ fm for central, $b =$ 5–9 fm for midcentral, and $b =$ 9–15 fm for peripheral collisions have been used.

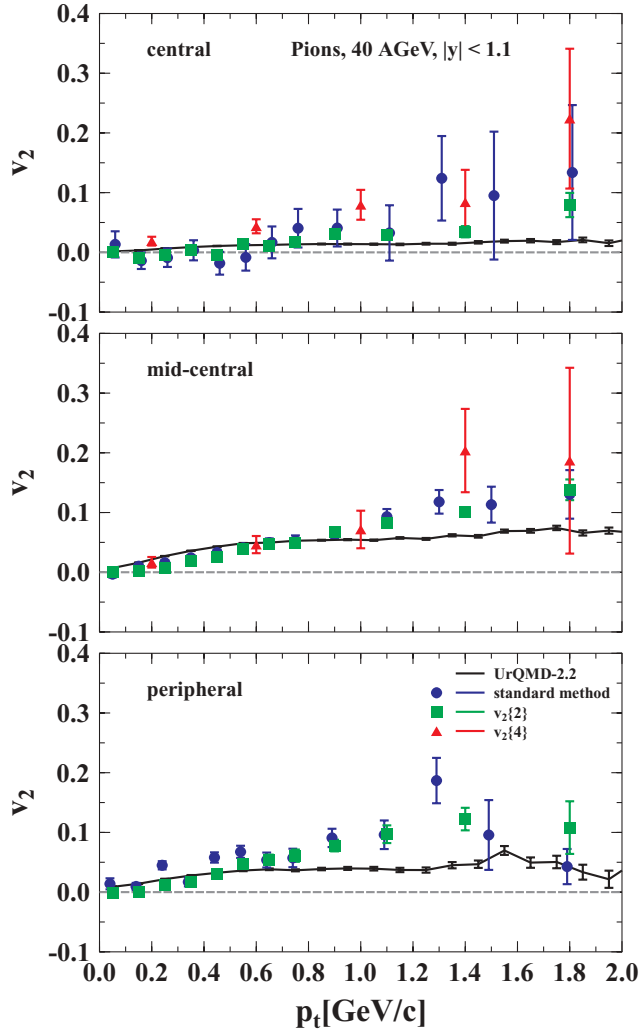

FIG. 23. (Color online) Elliptic flow of pions in Pb+Pb collisions at $E_{\rm lab} = 160A$ GeV with $|y| < 1.1$. UrQMD calculations are depicted with black lines. The symbols are NA49 data from different analysis methods. The standard method (circles), cumulant method of order 2 (squares), and cumulant method of order 3 (triangles) are depicted. The 12.5% most central collisions are labeled as central, the centrality 12.5%–33.5% as midcentral, and 33.5%–100% as peripheral. For the model calculations the corresponding impact parameters of $b \leqslant 3.4$ fm for central, $b =$ 5–9 fm for midcentral, and $b =$ 9–15 fm for peripheral collisions have been used.

with increasing transverse momentum because the larger the momentum of the particle the earlier it escapes the collision zone [53]. These high-energy particles carry the signal of the very early stage of the collision where the coordinate space asymmetry is most pronounced [23].

The elliptic flow of protons at $E_{\rm lab} = 160A$ GeV (Fig. 24) in central collisions looks similar to that at $40A$ GeV. There is a smooth increase from zero at $p_t = 0$ to about 2% at $p_t =$ 2 GeV/c. The underestimation of the flow by the transport model calculations at higher energies is visible in the results for midcentral and peripheral collisions at high p_t. At low p_t the calculations are in line with the data.

For pion elliptic flow at $160A$ GeV (Fig. 25) the picture is very similar to the plot of the proton flow at this energy.

The predictions for the transverse-momentum dependence of proton elliptic flow at $E_{\rm lab} = 20A$ GeV and $E_{\rm lab} =$ $30A$ GeV (Fig. 26) have mostly the same shape as the calculations at $40A$ GeV.

The elliptic flow of pions at 20 and $30A$ GeV shown in Fig. 27 are also similar to the calculations for the pion elliptic flow at $40A$ GeV. But there is a difference for peripheral collisions. At the higher energy there is a lower value than for the lower energy.

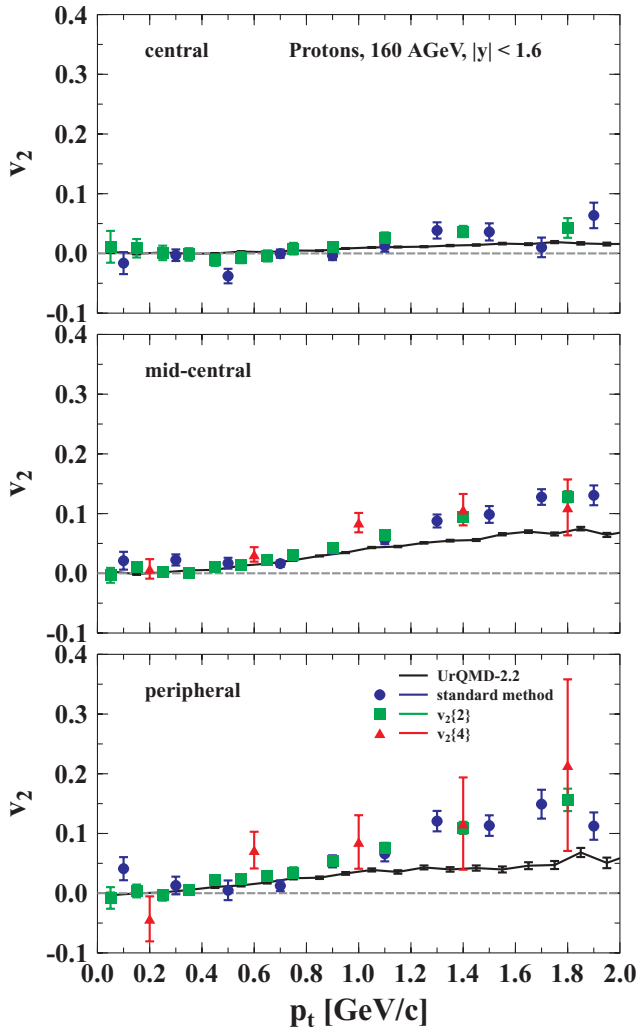

FIG. 24. (Color online) Elliptic flow of protons in Pb+Pb collisions at $E_{\text{lab}} = 40A$ GeV with $|y| < 1.6$. UrQMD calculations are depicted with black lines. The symbols are NA49 data from different analysis methods. The standard method (circles), cumulant method of order 2 (squares), and cumulant method of order 3 (triangles) are depicted. The 12.5% most central collisions are labeled as central, the centrality 12.5%–33.5% as midcentral, and 33.5%–100% as peripheral. For the model calculations the corresponding impact parameters of $b \leqslant 3.4$ fm for central, $b = 5$–9 fm for midcentral, and $b = 9$–15 fm for peripheral collisions have been used.

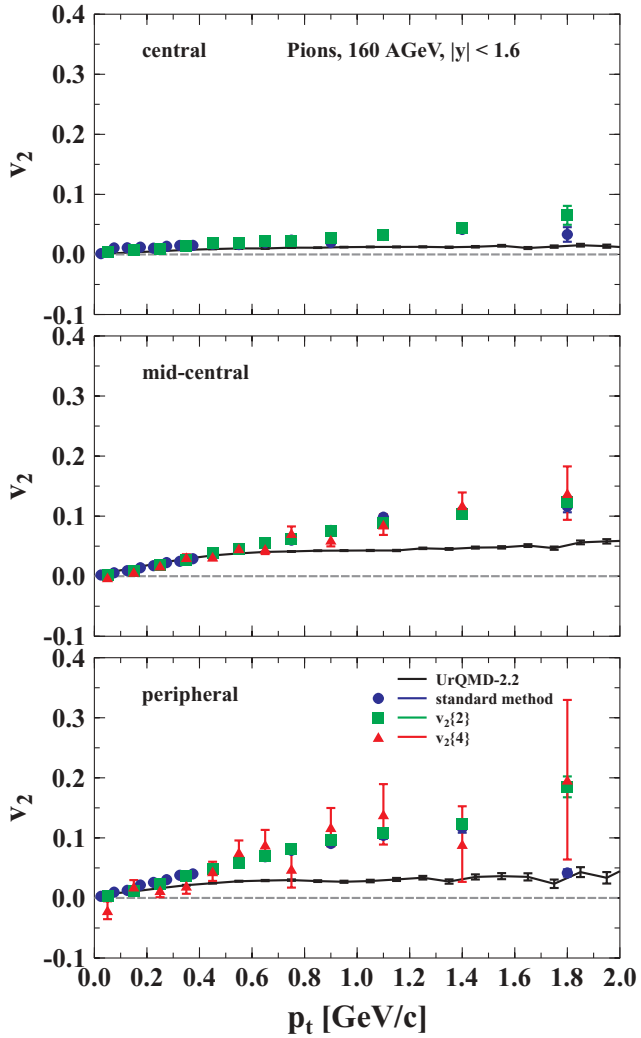

FIG. 25. (Color online) Elliptic flow of pions in Pb+Pb collisions at $E_{\text{lab}} = 40A$ GeV with $|y| < 1.6$. UrQMD calculations are depicted with black lines. The symbols are NA49 data from different analysis methods. The standard method (circles), cumulant method of order 2 (squares), and cumulant method of order 3 (triangles) are depicted. The 12.5% most central collisions are labeled as central, the centrality 12.5%–33.5% as midcentral, and 33.5%–100% as peripheral. For the model calculations the corresponding impact parameters of $b \leqslant 3.4$ fm for central, $b = 5$–9 fm for midcentral, and $b = 9$–15 fm for peripheral collisions have been used.

C. Excitation function

The excitation function of charged particle elliptic flow is compared to data over a wide energy range (Fig. 28), i.e., from $E_{\text{lab}} = 90A$ MeV to $\sqrt{s_{NN}} = 200$ GeV. The squeeze-out effect at low energies and the change to in-plane emission at higher energies is nicely observed in the excitation function. The symbols indicate the data for charged particles from different experiments. Note however, that in the low energy regime there are only experimental data points for protons. For beam energies below $2A$ GeV most of the charged particles are also protons because there is not enough energy to produce many new particles. Going to higher energies the elliptic flow of pions and charged particles are very similar. The rapidity cut of $|y| < 0.1$ has been used for the whole energy range despite the fact that the data at higher energies is within $|y| < 0.5$. This has been done to avoid too much changes in the parameters and this choice gives reasonable results over the whole energy range. We have checked that the results at higher energies are not affected by the choice of this narrower rapidity window.

At low energies $E_{\text{beam}} \sim 0.1$–$6\,A$ GeV the squeeze-out effect, i.e., the elliptic flow out of plane, is clearly seen in

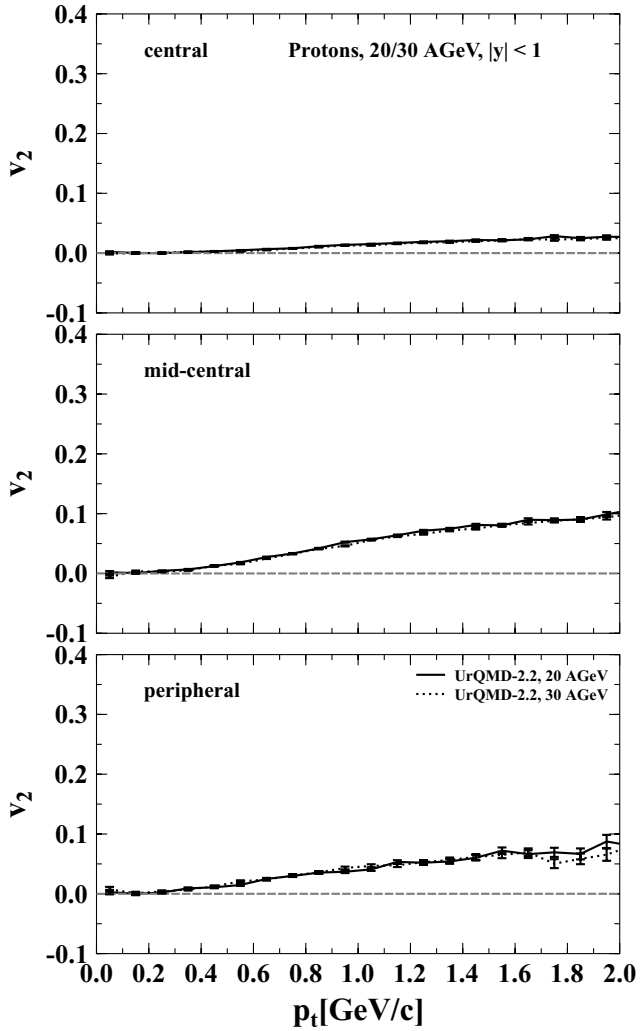

FIG. 26. Elliptic flow of protons in Pb+Pb collisions at $E_{\rm lab} = 20A$ GeV and $E_{\rm lab} = 30A$ GeV with $|y| < 1$. UrQMD calculations for $20A$ GeV are depicted with solid lines, whereas the results for $30A$ GeV are depicted by dashed lines. Impact parameters of $b \leqslant 3.4$ fm for central, $b = 5$–9 fm for midcentral, and $b = 9$–15 fm for peripheral collisions have been used.

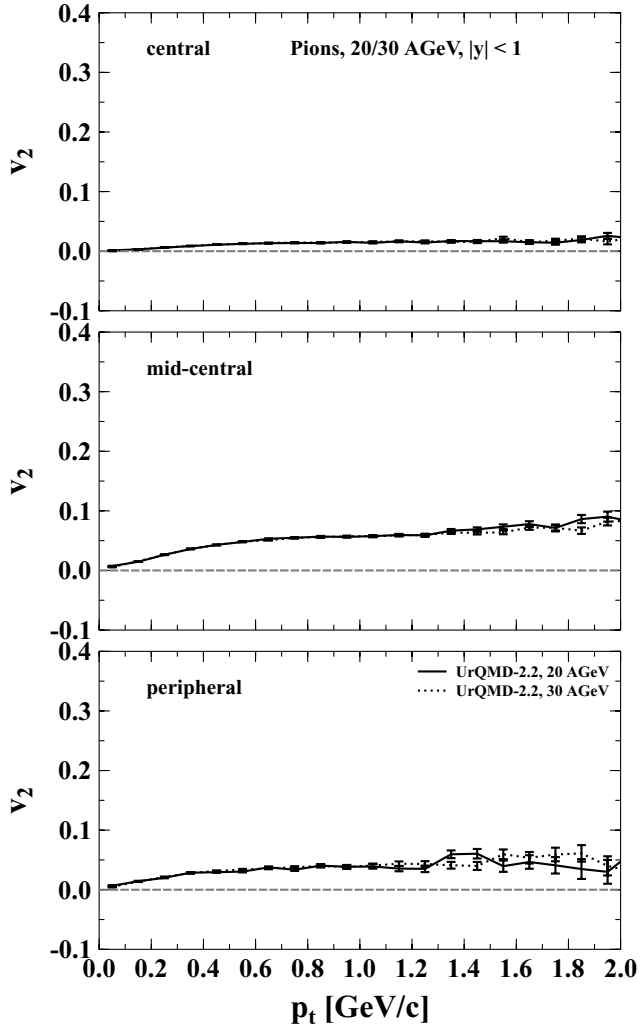

FIG. 27. Elliptic flow of pions in Pb+Pb collisions at $E_{\rm lab} = 20A$ GeV and $E_{\rm lab} = 30A$ GeV with $|y| < 1$. UrQMD calculations for $20A$ GeV are depicted with solid lines, whereas the results for $30A$ GeV are depicted by dashed lines. Impact parameters of $b \leqslant 3.4$ fm for central, $b = 5$–9 fm for midcentral, and $b = 9$–15 fm for peripheral collisions have been used.

the data as well as in the calculations, especially when the mean field is considered. At such energies, it is well known that both the mean field and the two-body collision are equally important to reproduce quantitatively the experimental results [63–65]. In this article we adopt a hard equation of state with momentum dependence (HM-EoS) that was updated recently in UrQMD model [50]. Meanwhile, the two-body scattering in heavy-ion collisions might be modified by the nuclear medium. To consider (partly) the medium effect, the nucleon-nucleon elastic scattering cross sections are modified to depend on the nuclear density, the isospin-asymmetry and the two-nucleon relative momentum, in addition to the center-of-mass energy of two nucleons. This treatment was investigated based on the relativistic Dirac-Brueckner-Hartree-Fock (DBHF) theory as well as the relativistic mean-field (RMF) theory, please see Ref. [51] for details. Here we show the calculation results with the HM-EoS and with the DBHF-like medium modification on nucleon-nulceon elastic cross sections (HMw) [51].

In the SPS regime the model calculations are quite in line with the data, especially with the NA49 results. Above $E_{\rm lab} = 160A$ GeV the calculation underestimates the elliptic flow. At the highest RHIC energy there are about 5% flow in the data, whereas the model calculation provides only half of this value. This can be explained by assuming a lack of pressure in the transport model at these energies.

In Fig. 29 the excitation function of elliptic flow of nucleons is presented. The rapidity cut of $|y| < 0.1$ has been used because this is the appropriate one to compare with the data at lower energies. Due to this cut now also the calculation in the cascade mode (without nuclear potential) reaches negative

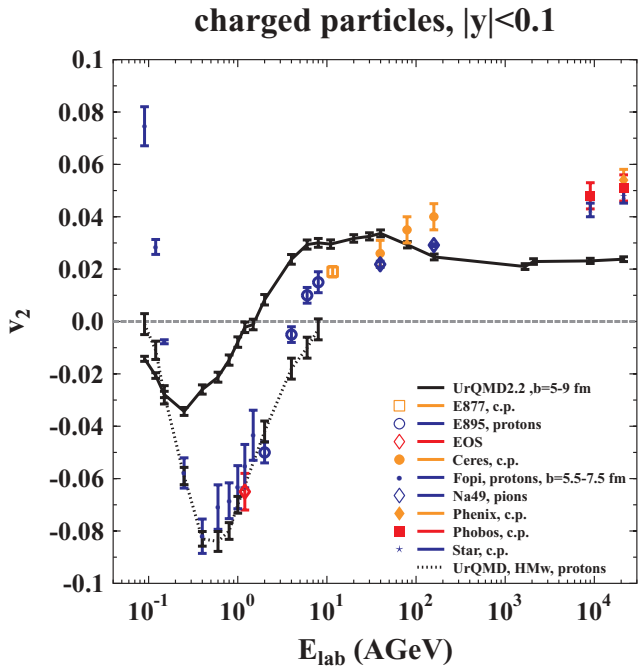

FIG. 28. (Color online) The calculated energy excitation function of elliptic flow of charged particles in Au+Au/Pb+Pb collisions in midcentral collisions ($b = 5$–9 fm)with $|y| < 0.1$(full line). This curve is compared to data from different experiments for midcentral collisions. For E895 [54,55] and FOPI [56] there is the elliptic flow of protons and for NA49 [11] it is the elliptic flow of pions. For E877, CERES [57–59], PHENIX [60], PHOBOS [61], and STAR [62] there is data for the charged particle flow. The dotted line in the low-energy regime depicts UrQMD calculations with the mean field [51].

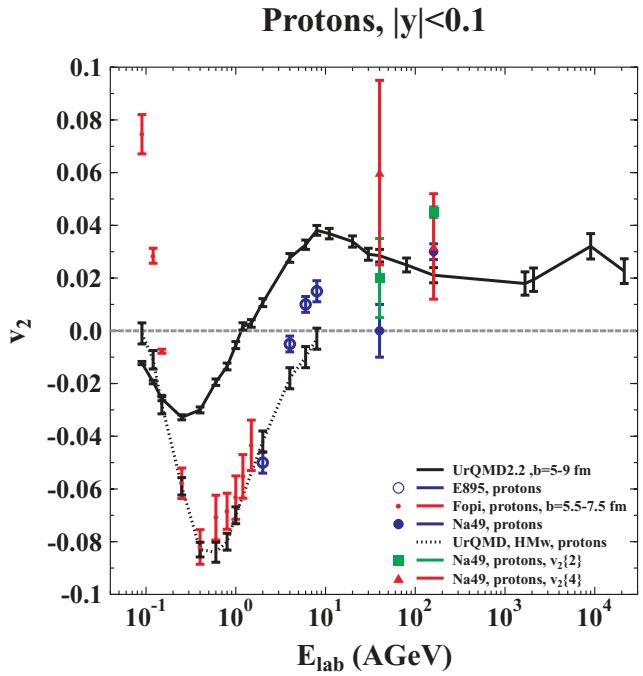

FIG. 29. (Color online) The calculated energy excitation function of elliptic flow of protons in Au+Au/Pb+Pb collisions in midcentral collisions ($b = 5$–9 fm)with $|y| < 0.1$ (full line). This curve is compared to data from different experiments for midcentral collisions. For E895 [54,55], FOPI [56], and NA49 [11] there is the elliptic flow of protons. The dotted line in the low energy regime depicts UrQMD calculations with included nuclear potential.

values at low energies. With included potential the model is in line with experimental data. The UrQMD result in the SPS energy range lies in between the NA49 measurement of elliptic flow of protons. These values have been extracted from the differential plots of elliptic flow over rapidity for midcentral collisions discussed above in this article.

The observed proton flow v_2 below $\sim 5A$ GeV is smaller than zero, which corresponds to the squeeze-out predicted by hydrodynamics long ago [4,5,66–69]. At higher energies, 10 to 160A GeV, an increase of the flow v_2 to a maximum around $E_{\text{lab}} = 10A$ GeV followed by a decrease to about 2% and a saturation is predicted from the string-hadronic transport model. In fact, the 158A GeV data of the NA49 Collaboration suggest that a smooth increase proceeds between AGS and SPS.

The "collapse" of v_2 (strong negative value) for protons around midrapidity at 40A GeV is only pronounced in the standard method data. The UrQMD calculations, without a phase transition, show a robust 3% flow of protons. One cannot say anything about a clear underestimation at high energies in this case because integrated proton flow data at RHIC is still not available.

VII. SUMMARY

We have compared UrQMD calculations to recent NA49 data. In general, a good agreement between data and calculation is found. There seem to be systematic uncertainties in the measurement method looking at the different results. For example for the directed flow data the effect of momentum conservation on the flow data can be seen. The slope around midrapidity of the rapidity distributions of proton directed flow becomes negative around $E_{\text{lab}} = 40A$ GeV. This cannot be reproduced by the transport model calculations. The excitation function of elliptic flow shows strong negative flow at low energies—the "squeeze-out" effect—which can quantitatively only be reproduced by including a nuclear potential in the calculation. At high energies we observed an underestimation of the elliptic flow of charged particles in the present model. This can possibly be explained by assuming a lack of pressure in the early stage of the collisions at high energies. It will be very interesting to see what happens in the lower-energy regime (20/30 A GeV) when high-quality CBM-FAIR data become accessible.

ACKNOWLEDGMENTS

We are grateful to the Center for the Scientific Computing (CSC) at Frankfurt for the computing resources. The authors

thank Alexander Wetzler for helpful and stimulating discussions. Q. Li thanks the Alexander von Humboldt-Stiftung for financial support. This work was supported by GSI and BMBF.

[1] *Proceedings of the Quark Matter 2005*, Budapest, Hungary [Nucl. Phys. **A774**, 1 (2006)].
[2] W. Scheid, J. Hofmann, and W. Greiner, In *Proceedings* (Lawrence Berkeley Lab Lbl-3675, Berkeley, 1974), pp. 1–50.
[3] H. Stöcker, J. A. Maruhn, and W. Greiner, Z. Phys. A **290**, 297 (1979).
[4] J. Hofmann, H. Stöcker, U. W. Heinz, W. Scheid, and W. Greiner, Phys. Rev. Lett. **36**, 88 (1976).
[5] H. Stöcker and W. Greiner, Phys. Rep. **137**, 277 (1986).
[6] Z. Fodor and S. D. Katz, J. High Energy Phys. 03 (2002) 014.
[7] Z. Fodor, S. D. Katz, and K. K. Szabo, Phys. Lett. **B568**, 73 (2003).
[8] L. P. Csernai and D. Rohrich, Phys. Lett. **B458**, 454 (1999).
[9] H. Stöcker, Nucl. Phys. **A750**, 121 (2005).
[10] H. Stöcker, E. L. Bratkovskaya, M. Bleicher, S. Soff, and X. Zhu, J. Phys. G **31**, S929 (2005).
[11] C. Alt *et al.* (NA49 Collaboration), Phys. Rev. C **68**, 034903 (2003).
[12] M. Bleicher *et al.*, J. Phys. G **25**, 1859 (1999).
[13] S. A. Bass *et al.*, Prog. Part. Nucl. Phys. **41**, 225 (1998).
[14] B. Andersson, G. Gustafson, and B. Nilsson-Almqvist, Nucl. Phys. **B281**, 289 (1987).
[15] B. Nilsson-Almqvist and E. Stenlund, Comput. Phys. Commun. **43**, 387 (1987).
[16] T. Sjostrand, Comput. Phys. Commun. **82**, 74 (1994).
[17] M. Belkacem *et al.*, Phys. Rev. C **58**, 1727 (1998).
[18] L. V. Bravina *et al.*, Phys. Rev. C **60**, 024904 (1999).
[19] E. L. Bratkovskaya, M. Bleicher, M. Reiter, S. Soff, H. Stocker, M. Van Leeuwen, S. A. Bass, and W. Cassing, Phys. Rev. C **69**, 054907 (2004).
[20] M. Bleicher, E. Bratkovskaya, S. Vogel, and X. Zhu, J. Phys. G **31**, S709 (2005).
[21] L. A. Winckelmann *et al.*, Nucl. Phys. **A610**, 116C (1996).
[22] M. Bleicher *et al.*, Phys. Lett. **B447**, 227 (1999).
[23] Y. Lu *et al.*, J. Phys. G: Nucl. Part. Phys. **32**, 1121 (2006).
[24] X. Zhu, M. Bleicher, and H. Stöcker, J. Phys. G **32**, 2181 (2006).
[25] X. Zhu, M. Bleicher, and H. Stöcker, Phys. Rev. C **72**, 064911 (2005).
[26] P. F. Kolb, J. Sollfrank, and U. Heinz, Phys. Rev. C **62**, 054909 (2000).
[27] D. H. Rischke, Y. Pursun, J. A. Maruhn, H. Stöcker, and W. Greiner, Heavy Ion Phys. **1**, 309 (1995).
[28] M. Bleicher and J. Aichelin, Phys. Lett. **B612**, 201 (2005).
[29] S. Soff, S. A. Bass, M. Bleicher, H. Stöcker, and W. Greiner, arXiv:nucl-th/9903061.
[30] H. Sorge, Phys. Rev. Lett. **82**, 2048 (1999).
[31] J. Y. Ollitrault, Phys. Rev. D **46**, 229 (1992).
[32] C. M. Hung and E. V. Shuryak, Phys. Rev. Lett. **75**, 4003 (1995).
[33] D. H. Rischke, Nucl. Phys. **A610**, 88C (1996).
[34] H. Sorge, Phys. Rev. Lett. **78**, 2309 (1997).
[35] H. Heiselberg and A. M. Levy, Phys. Rev. C **59**, 2716 (1999).
[36] J. Brachmann, S. Soff, A. Dumitru, H. Stocker, J. A. Maruhn, W. Greiner, L. V. Bravina, and D. H. Rischke, Phys. Rev. C **61**, 024909 (2000).
[37] J. Brachmann, A. Dumitru, H. Stöcker, and W. Greiner, Eur. Phys. J. A **8**, 549 (2000).
[38] B. Zhang, M. Gyulassy, and C. M. Ko, Phys. Lett. **B455**, 45 (1999).
[39] M. Bleicher and H. Stöcker, Phys. Lett. **B526**, 309 (2002).
[40] A. M. Poskanzer and S. A. Voloshin, Phys. Rev. C **58**, 1671 (1998).
[41] N. Borghini, P. M. Dinh, and J. Y. Ollitrault, Phys. Rev. C **62**, 034902 (2000).
[42] Y. V. Kovchegov and K. L. Tuchin, Nucl. Phys. **A708**, 413 (2002).
[43] P. M. Dinh, N. Borghini, and J. Y. Ollitrault, Phys. Lett. **B477**, 51 (2000).
[44] N. Borghini, P. M. Dinh, and J. Y. Ollitrault, Phys. Rev. C **63**, 054906 (2001).
[45] N. Borghini, P. M. Dinh, and J. Y. Ollitrault, Phys. Rev. C **64**, 054901 (2001).
[46] M. Miller and R. Snellings, nucl-ex/0312008.
[47] N. Borghini, P. M. Dinh, J. Y. Ollitrault, A. M. Poskanzer, and S. A. Voloshin, Phys. Rev. C **66**, 014901 (2002).
[48] N. Borghini, P. M. Dinh, and J. Y. Ollitrault, Phys. Rev. C **66**, 014905 (2002).
[49] H. Liu *et al.* (E895 Collaboration), Phys. Rev. Lett. **84**, 5488 (2000).
[50] Q. Li, Z. Li, S. Soff, M. Bleicher, and H. Stöcker, J. Phys. G: Nucl. Part. Phys. **32**, 151 (2006).
[51] Q. Li, Z. Li, S. Soff, M. Bleicher, and H. Stöcker, J. Phys. G: Nucl. Part. Phys. **32**, 407 (2006).
[52] J. Brachmann, Ph.D. thesis, JW Goethe Universität, 2000.
[53] S. A. Bass, C. Hartnack, H. Stöcker, and W. Greiner, Phys. Rev. C **50**, 2167 (1994).
[54] C. Pinkenburg *et al.* (E895 Collaboration), Phys. Rev. Lett. **83**, 1295 (1999).
[55] P. Chung *et al.* (E895 Collaboration), Phys. Rev. C **66**, 021901 (2002).
[56] A. Andronic *et al.* (FOPI Collaboration), Phys. Lett. **B612**, 173 (2005).
[57] K. Filimonov *et al.* (CERES/NA45 Collaboration), arXiv:nucl-ex/0109017.
[58] J. Slivova (CERES/NA45 Collaboration), Nucl. Phys. **A715**, 615 (2003).
[59] S. I. Esumi, J. Slivova, and J. Milosevic for CERES Collaboration SFIN, year XV, Series A: Conferences, No. A2 (2002).
[60] S. Esumi (PHENIX Collaboration), Nucl. Phys. **A715**, 599 (2003).
[61] S. Manly *et al.* (PHOBOS Collaboration), Nucl. Phys. **A715**, 611 (2003).

[62] R. L. Ray (STAR Collaboration), Nucl. Phys. **A715**, 45 (2003).
[63] P. Danielewicz, Nucl. Phys. **A661**, 82 (1999).
[64] P. Danielewicz, R. A. Lacey, P. B. Gossiaux, C. Pinkenburg, P. Chung, J. M. Alexander, and R. L. McGrath, Phys. Rev. Lett. **81**, 2438 (1998).
[65] Q. B. Pan and P. Danielewicz, Phys. Rev. Lett. **70**, 2062 (1993) [Erratum-*ibid*. **70**, 3523 (1993)].
[66] J. Hofmann, H. Stöcker, W. Scheid, and W. Greiner, *Report of the Workshop on BeV/Nucleon Collisions of Heavy Ions—How and Why, Bear Mountain, New York, November 29–December 1* (BNL-AUI 1975)(1974).
[67] H. Stöcker, J. A. Maruhn, and W. Greiner, Phys. Rev. Lett. **44**, 725 (1980).
[68] H. Stöcker, J. Hofmann, J. A. Maruhn, and W. Greiner, Prog. Part. Nucl. Phys. **4**, 133 (1980).
[69] H. Stöcker, L. P. Csernai, G. Graebner, G. Buchwald, H. Kruse, R. Y. Cusson, J. A. Maruhn, and W. Greiner, Phys. Rev. C **25**, 1873 (1982).